CORA Cork Open Research Archive
Cartlann Taighde Oscailte Chorcaí

Title	Field-induced reversible insulator-to-metal transition and the onset of ferroelectricity in molybdenum trioxide films
Authors	Dragoman, Mircea;Modreanu, Mircea;Sheehan, Brendan;Vulpe, Silviu;Romanitan, Cosmin;Aldrigo, Martino;Dinescu, Adrian;Serban, Andreea Bianca;Dragoman, Daniela
Publication date	2023-06-01
Original Citation	Dragoman, M., Modreanu, M., Sheehan, B., Vulpe, S., Romanitan, C., Aldrigo, M., Dinescu, A., Serban, A. B. and Dragoman, D. (2023) 'Field-induced reversible insulator-to-metal transition and the onset of ferroelectricity in molybdenum trioxide films', Journal of Applied Physics, 133(21), 215101 (11pp). doi: 10.1063/5.0151117
Type of publication	Article (peer-reviewed)
Link to publisher's version	10.1063/5.0151117
Rights	© 2023, the Authors. Published under an exclusive license by AIP Publishing. This article may be downloaded for personal use only. Any other use requires prior permission of the author and AIP Publishing. This article appeared as: Dragoman, M., Modreanu, M., Sheehan, B., Vulpe, S., Romanitan, C., Aldrigo, M., Dinescu, A., Serban, A. B. and Dragoman, D. (2023) 'Field-induced reversible insulator-to-metal transition and the onset of ferroelectricity in molybdenum trioxide films', Journal of Applied Physics, 133(21), 215101 (11pp), doi: 10.1063/5.0151117, and may be found at: https://doi.org/10.1063/5.0151117
Download date	2026-11-03 08:43:27
Item downloaded from	https://hdl.handle.net/10468/14589



University College Cork, Ireland
Coláiste na hOllscoile Corcaigh

ACCEPTED MANUSCRIPT
Journal of Applied Physics
AIP Publishing
This is the author's peer reviewed, accepted manuscript. However, the online version of record will be different from this version once it has been copyedited and typeset.
PLEASE CITE THIS ARTICLE AS DOI: 10.1063/5.0151117

Field-induced reversible insulator-to-metal transition and the onset of the ferroelectricity in molybdenum trioxide films

Mircea Dragoman[1*], Mircea Modreanu[2], Brendan Sheehan[2], Silviu Vulpe[1], Cosmin Romanitan[1], Martino Aldrigo[1], Adrian Dinescu[1], Andreea Bianca Serban[3], Daniela Dragoman[4,5]

[1]National Institute for Research and Development in Microtechnologies (IMT Bucharest), Erou Iancu Nicolae Street 126A, 077190 Voluntari (Ilfov), Romania

[2]Tyndall National Institute-University College Cork, Lee Maltings, Dyke Parade, Cork, Ireland

[3]Extreme Light Infrastructure-Nuclear Physics (ELI-NP), "Horia Hulubei" National R&D Institute for Physics and Nuclear Engineering (IFIN-HH), Magurele, Ilfov 077125, Romania

[4]Univ. of Bucharest, Physics Faculty, P.O. Box MG-11, 077125 Bucharest, Romania

[5]Academy of Romanian Scientists, Str. Ilfov, Nr. 3, 050044 Bucharest, Romania

*Corresponding author: mircea.dragoman@imt.ro

Abstract

This paper presents the experimental evidence of the reversible insulator-metal transition (IMT) in thin-film amorphous molybdenum trioxide (MoO_3) induced by electric fields of just a few volts. The presence of oxygen vacancies in MoO_3 is considered to play a significant role in the reported reversible IMT. The oxygen vacancies impact not only the MoO_3 stoichiometry but also the optical bandgap. The subthreshold slope for IMT in 10nm-thick MoO_3-based devices is 48.3 mV/decade, which represents a transition from an insulator to a metallic state, and the electric field threshold for such transition was found to be equal to 0.034 V/Å.

ACCEPTED MANUSCRIPT

This is the author's peer reviewed, accepted manuscript. However, the online version of record will be different from this version once it has been copyedited and typeset.
PLEASE CITE THIS ARTICLE AS DOI: 10.1063/5.0151117

Journal of Applied Physics
AIP Publishing

Following the IMT in MoO_3, there are 6 orders of magnitude differences between the resistivity of the insulator state (27.5 MΩ at -9 V) and metallic state (80 Ω between +5 and +9 V). In addition, we reported the stabilization of a nanocrystalline hexagonal MoO_3 (h-MoO_3) phase in thicker MoO_3 (150nm-thick) in the presence of the oxygen vacancies that behaves as a wide bandgap (3.1 eV) ferroelectric semiconductor with a coercive field of about 50 kV/cm, a saturation polarization of about 30 μC/cm^2, and a remanent polarization of about 10 μC/cm^2. This ferroelectricity in nanocrystalline h-MoO_3 (150nm-thick) remains stable even after 8 months of storage of the sample in ambient conditions, with the remanent polarization increasing up to 20 μC/cm^2. These are unexpected results from MoO_3.

1. Introduction

The insulator-metal transition (IMT), which is typically described by a large change in electrical conductivity with external stimuli, has been widely observed and intensively investigated over the last few decades. It was first described by N. F. Mott in 1968 [1] and atomically thin transition metal dichalcogenides (TMDs) [2] are the latest IMT materials under scrutiny, with applications in microwaves devices and components (e.g., antennas and switches). In particular, the control of the IMT phenomenon through an applied electric field may open new applications in multifunctional devices such as memory, optical modulators, and artificial synaptic networks. Among the TMD materials we can mention molybdenum disulphide (MoS_2), which (in its monolayer form) is the most studied atomically thin material after graphene. Monolayer MoS_2 is a direct bandgap *n*-type semiconductor with a bandgap of ~1.9 eV, while the bandgap decreases as the number of monolayers increases, its bulk counterpart being an indirect semiconductor with a bandgap of ~1.2 eV. There are two types of induced IMT: an irreversible or structural phase transition, with re-arrangement of either sulph or molybdenum atoms, and a reversible phase transition (e.g., few-layer MoS_2 under an applied

ACCEPTED MANUSCRIPT
Journal of Applied Physics
AIP Publishing
This is the author's peer reviewed, accepted manuscript. However, the online version of record will be different from this version once it has been copyedited and typeset.
PLEASE CITE THIS ARTICLE AS DOI: 10.1063/5.0151117

pressure or via electrostatic gating in a field-effect device). However, there still exist difficulties in the growth of high-quality MoS_2 at the wafer level; furthermore, MoS_2 exhibits a low mobility with respect to other semiconductors and is subject to oxidation with the subsequent creation of molybdenum oxides (MO_x) compounds. For this reason, it was straightforward to investigate new molybdenum-based compounds able to overcome the limitations of MoS_2.

Molybdenum oxides are a class of transitional metal oxides with numerous applications in electronics, catalysis, sensors, energy-storage units, field emission devices, super-conductors, thermal materials, biosystems, chromogenics, and electrochromic systems [3-8]. Molybdenum oxides are amongst the most versatile metal oxides due to their unique electrical, structural, chemical, and optical properties, which depend on the oxidation state of Mo and the degree of crystallinity. They are found in various stoichiometries, ranging from stoichiometric molybdenum trioxide (MoO_3) to more conducting reduced oxides in the form of MoO_{3-x} ($0<x<2$) and eventually semi-metallic molybdenum dioxide (MoO_2).

MoO_3 is a van der Waals semiconductor with the most stable crystalline polymorph being the α-MoO_3, which has an orthorhombic crystal lattice consisting of double layers of MoO_6 octahedra as a framework. Recently, it has been receiving significant attention thanks to its ability to support highly anisotropic phonon polaritons (PhPs)—infrared (IR) light coupled to lattice vibrations—offering an unprecedented platform for controlling the energy flow at the nanoscale [3, 4]. Conversely, MoO_2 crystallizes in a distorted rutile phase and presents a metallic band structure. Its metallicity arises from the presence of Mo_{3d} orbitals near the Fermi level [5, 6]. MoO_3 is a semiconducting metal oxide having a wide bandgap (3.2 eV for the fully stoichiometric MoO_3). However, the bandgap can be reduced by oxygen vacancies in the non-stoichiometric version MoO_{3-x}. The growth methods and many applications of MoO_3, such as chromic devices, photocatalysis, solar cell and emitting diodes, photodetectors, thermoelectric devices, and sensors are reviewed in Ref. [7].

ACCEPTED MANUSCRIPT
Journal of Applied Physics
AIP Publishing
This is the author's peer reviewed, accepted manuscript. However, the online version of record will be different from this version once it has been copyedited and typeset.
PLEASE CITE THIS ARTICLE AS DOI: 10.1063/5.0151117

The discovery of atomically thin materials, such as graphene or TMDs, has triggered the research of thin-film oxides and their applications in electronics and optoelectronics. MoO_3 is a van der Waals semiconductor that attracted a great deal of interest as a new class of thin-film materials [8-10].

Although the applications of MoO_3 in nanoelectronics are scarce, they are remarkable. For example, a field-effect transistor (FET) based on thin-film MoO_{3-x} has been already reported [11]. Thin-film MoO_{3-x} flakes have a thickness of 11 nm, i.e., the thickness of eight atomic layers, with each atomic layer having a thickness of 1.4 nm. The room-temperature carrier mobility attains a value of 1100 $cm^2/V{\cdot}s$, which is comparable with the mobility of silicon (Si)-based CMOS FETs. A similar result was obtained using ink of MoO_{3-x} nanoflakes, in which case the mobility is 600 $cm^2/V{\cdot}s$ [12]. These high mobility values outperform the mobility of any FET based on transition metal dichalcogenides such as MoS_2. However, the drain currents are maximum a few μA, but the drain current on/off ratio is very high, i.e., 10^5. Similar results are obtained in ultrathin indium tin oxide (ITO) short-channel FETs, where the mobility is equal to 60 $cm^2/V{\cdot}s$ [13]. Such short-channel ITO FETs, with ITO channel lengths in the range of 40-60 nm and ITO thickness in the range of 5-10 nm, can work at microwaves up to 5 GHz [14]. Since the mobility of MoO_{3-x} is at least one magnitude bigger than ITO, it is expected that MoO_{3-x} FETs will be able to work beyond 10 GHz.

The insulator-to-metal phase transition in MoO_{3-x} induced by an electric field produces an on and an off state of the current similar to other FETs; however, the physical origin of IMT is different for MoO_{3-x} and recently Y. Ogawa et al. [15] have attributed it to the reversible transition between an amorphous state and a crystalline state. In this work of Y. Ogawa et al., the thickness of the MoO_{3-x} film was quite large, i.e., 450 nm, and represents a limiting factor for the reversible transitions between amorphous and crystalline states. In addition, the reported current is rather low, 0.1 mA.

ACCEPTED MANUSCRIPT
Journal of Applied Physics
AIP Publishing
This is the author's peer reviewed, accepted manuscript. However, the online version of record will be different from this version once it has been copyedited and typeset.
PLEASE CITE THIS ARTICLE AS DOI: 10.1063/5.0151117

We are reporting here the investigation of the reversible insulator-to-metal phase transition controlled by an applied electric field in MoO_{3-x} thin-films with thicknesses of 10 nm, 15 nm, and 25 nm or, equivalently, of 8, 12, and 20 atomic layers, respectively. For this study, the vertical diodes in the classical configuration metal-isolator-semiconductor (MIS) have been fabricated for each of these MoO_{3-x} thin films. We report here a reproducible reversible IMT with an on/off current ratio of at least 10^5 (the on/off current ratio could be even higher as we have limited the current at 10 mA to avoid the breakdown of the devices). The role of oxygen vacancies in controlling the reversible insulator-to-metal phase transition in thin-film MoO_{3-x} is investigated here. Moreover, we are reporting here that when growing thicker MoO_{3-x} (150 nm) films, we can observe the occurrence of ferroelectric phenomena in MoO_{3-x} that remains present even 8 months after the first measurements. We are investigating here the role played by oxygen vacancies in the stabilization of a nanocrystalline hexagonal MoO_3 phase (h-MoO_3) in 150nm-thick MoO_{3-x} that is proposed to be linked to the observed ferroelectric properties. In this respect, the results expand the range of materials with ferroelectric behavior induced by oxygen vacancies, like in the case of doped hafnium oxides and nitrogen-doped nickel oxides. This opens opportunities for the development of new ferroelectric devices based on MoO_3, such as non-volatile memory, piezoelectric sensors, and actuators. Further research will explore the potential of MoO_3 as a ferroelectric material in these and other applications.

Several characterization techniques, such as X-ray photoemission spectroscopy (XPS), spectroscopic ellipsometry (SE), UV-VIS-NIR optical spectrophotometry, and X-ray diffraction have been employed for in-depth study of the structural, chemical, and optical properties of MoO_{3-x} films.

2. Experimental details

Amorphous MoO_3 thin films were deposited at room temperature by e-beam evaporation using MoO_3 pellets (Pi-KEM 99.99% purity) in a Leybold SYRUS pro 710 on two types of

ACCEPTED MANUSCRIPT
Journal of Applied Physics
AIP Publishing
This is the author's peer reviewed, accepted manuscript. However, the online version of record will be different from this version once it has been copyedited and typeset.
PLEASE CITE THIS ARTICLE AS DOI: 10.1063/5.0151117

substrates, i.e., fused silica and *n*-type silicon. The nominal thickness of these MoO_3 films targeted both ultrathin films (10, 15, and 25 nm grown on Si) and thicker films (150nm grown on both Si and on fused silica substrate). The *n*-type Si (100) wafers were cleaned before the deposition using a standard RCA cleaning procedure. For the electrical measurements two approaches have been followed as shown in Fig. 1a: (i) n^{++} implantation of the backside of the *n*-type Si (100) substrates has been performed using a two-step implantation process, first the P implantation at a dose of 5×10^{13} cm^{-2} at 110 keV, then the As implantation at a dose of 6×10^{15} cm^{-2} at 110 keV, and this was followed by furnace annealing at 900°C for 1 hour in nitrogen and back-side metallization with 1µm-thick 1% Si-doped Al deposited by metal evaporation using a TEMESCAL tool (Fig. 1b); (ii) top-side metallization by metal evaporation of 5 nm Ti/100 nm Au. For the top electrical contacts, we used 5 nm Cr/100 nm Au deposited through a shadow mask by e-beam evaporation (TEMESCAL FC2000). The nominal MoO_{3-x} thickness was checked by using spectroscopic ellipsometry and X-ray reflectivity (XRR) and the results have been found to be in good agreement with a typical deviation from the nominal thickness of less than 10%. The cross-section of the devices fabricated on three distinct wafers for each MO_{3-x} thickness (10 nm, 15 nm, and 25 nm) used for studying field-induced phase transition are represented in Fig. 1a-c. In the end, up to 20 devices were fabricated for each wafer.

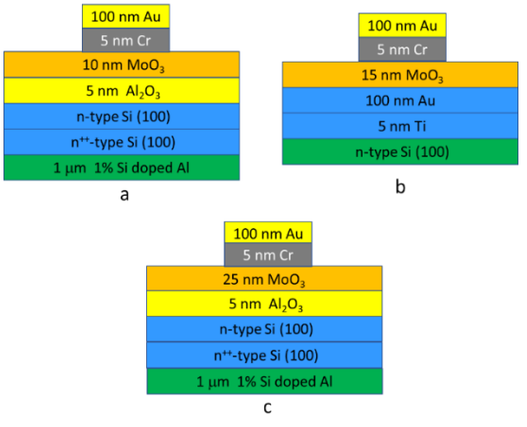


Fig. 1: Schematic cross-sections of MO_3 devices with a thickness of (a) 10 nm, (b) 15 nm, and (c) 25 nm.

ACCEPTED MANUSCRIPT
Journal of Applied Physics
AIP Publishing
This is the author's peer reviewed, accepted manuscript. However, the online version of record will be different from this version once it has been copyedited and typeset.
PLEASE CITE THIS ARTICLE AS DOI: 10.1063/5.0151117

The Grazing incidence X-ray diffraction (GI-XRD) pattern was recorded using a 9kW Rigaku SmartLab diffractometer, operated at 45 kV and 200 mA. The incidence angle of the source was fixed at 0.5°, while the detector scanned from 10 to 95°.

X-ray photoemission spectroscopy (XPS) spectra were recorded on a Sigma Surface Science photoelectron spectrometer equipped with a 160-mm hemispherical energy analyzer with a 1D detector (ASPECT). XPS measurements were performed using a polychromatic Mg Kα X-ray source at 1253.6 eV with a power of 300 W. The vacuum was maintained at ~2×10^{9} mbar. The diameter of analysis spot was 1.3 mm. Wide scan survey spectra were collected from -5 to 1200 eV (binding energy), using constant pass energy of 200 eV. The high-resolution spectra were recorded using a pass energy of 20 eV and a step of 0.1 eV. The XPS spectra were analysed by CasaXPS software using Shirley background determination. XPS measurements have been performed on two MoO_3 films with a nominal thickness of 10nm and 150 nm.

UV-VIS-NIR optical transmission measurements have been performed on 150nm-thick MoO_{3-x} film deposited on fused silica in normal incidence transmission configuration using a Perkin Elmer Lambda 950 double-beam spectrophotometer.

Spectroscopic ellipsometry has been performed on the 150nm-thick MoO_{3-x} ($MoO_{2.94}$) film deposited on Si and on the 10nm-thick MoO_{3-x} ($MoO_{2.96}$) deposited on 3nm-thick Al_2O_3/Si substrate. The measurements were performed at a 70-degree incidence using a Woollam M2000 ellipsometer in the UV-VIS-NIR spectral range. The collected ellipsometry data have been analysed considering a four-layer optical model, i.e., air/MoO_3/interfacial oxide/silicon as was described in a previous work [6]. For the ellipsometry data modelling Woollam's CompletEASE software was used. The dispersion of the complex dielectric function for the 150nm-thick $MoO_{2.94}$ and 10nm-thick $MoO_{2.96}$ was obtained in this way. The absorption coefficient, α, was derived from the extinction coefficient, k using the formula: $\alpha = \frac{4\pi k}{\lambda}$.

ACCEPTED MANUSCRIPT
Journal of Applied Physics
AIP Publishing
This is the author's peer reviewed, accepted manuscript. However, the online version of record will be different from this version once it has been copyedited and typeset.
PLEASE CITE THIS ARTICLE AS DOI: 10.1063/5.0151117

Sample cross sections (lamella) for analysis using Transmission Electron Microscopy (TEM) were prepared using a DualBeam focused ion beam (FIB) FEI Helios NanoLab 600i. A number of protective layers were formed over the area/surface of interest before FIB milling. Using electron-beam induced deposition, layers consisting of 50-100 nm of carbon and 300-500 nm of platinum were deposited within the DualBeam FIB. Finally, using ion-beam induced deposition, a 3.5µm-thick carbon layer was deposited on top. The lamella was prepared and lifted out onto a copper grid for TEM. Lamella thinning for electron transparency was carried out at 30 kV with a final polish at 5 kV (47 pA) to reduce the ion-beam induced damage. Micro-structural analysis was performed by means of a TEM equipment (Jeol 2100 transmission electron microscope; 200 kV) using a double tilt sample holder.

3. Results and discussion

X-ray photoemission spectroscopy

XPS was used to examine the chemical state and chemical composition of the surface species. The high-resolution Mo 3d spectra of the 10nm-thick MoO_3 and 150nm-thick MoO_3 films illustrated in Fig. 2 indicate two sharp peaks with a spin split of 3.1 eV and a peak ratio of 3:2. The positions of the main deconvoluted spin–orbit coupling Mo $3d_{5/2}$ and Mo $3d_{3/2}$ is assigned to the Mo^{6+} oxidation state located at 232.8 eV and 235.9 eV respectively. Furthermore, both samples, present a second doublet (Mo^{5+} oxidized state) that is required to obtain an accurate fit of the experimental data (Mo $3d_{5/2}$ at 231.5 eV, and Mo $3d_{3/2}$ at 234.6 eV). The presence of a small Mo^{5+} $3d_{5/2}$ is considered indicative of the presence of oxygen vacancies in MoO_3. The MoO_3 propensity to form oxygen vacancies has been often reported [6, 16] and has been theoretically investigated recently [17].

ACCEPTED MANUSCRIPT
Journal of Applied Physics
AIP Publishing
This is the author's peer reviewed, accepted manuscript. However, the online version of record will be different from this version once it has been copyedited and typeset.
PLEASE CITE THIS ARTICLE AS DOI: 10.1063/5.0151117

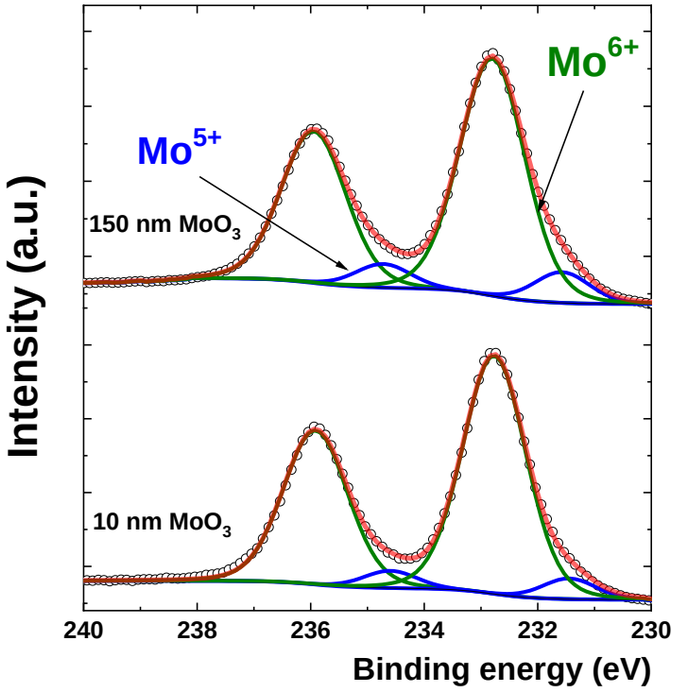


Fig. 2: High-resolution XPS spectra Mo 3d for the 10nm-thick and 150nm-thick MoO_3 films.

The experimental data is shown as open black circles, while the red curves are the sum of the deconvoluted components, i.e., Mo^{5+} and Mo^{6+} 3d.

The atomic ratio between Mo and O was found by using the formula from Ref. [18]. The Mo to O atomic ratio of the thin-film MoO_3 (10nm-thick) sample is 1:2.96, while the thicker MoO_3 (150nm-thick film) sample present a ratio of 1:2.94. The atomic concentration ratio of Mo^{6+} to Mo^{5+} is obtained to be about 13:1 for the 10nm-thick sample and about 9:1 for the 150nm-thick MoO_3 sample. Therefore, the results indicate that the e-beam evaporation of the MoO_3 leads to the formation of oxygen-deficient molybdenum trioxides film, with an oxygen deficiency increase of the thicker film. Furthermore, the XPS results indicate that MoO_3 films present a surface that is free from any elemental impurities.

Grazing incidence X-ray diffraction

ACCEPTED MANUSCRIPT
Journal of Applied Physics
AIP Publishing
This is the author's peer reviewed, accepted manuscript. However, the online version of record will be different from this version once it has been copyedited and typeset.
PLEASE CITE THIS ARTICLE AS DOI: 10.1063/5.0151117

In Fig. 3 are shown the GI-XRD patterns for MoO_3 thin films at different thickness: 10, 15, and 25 nm, as well for film (150 nm).

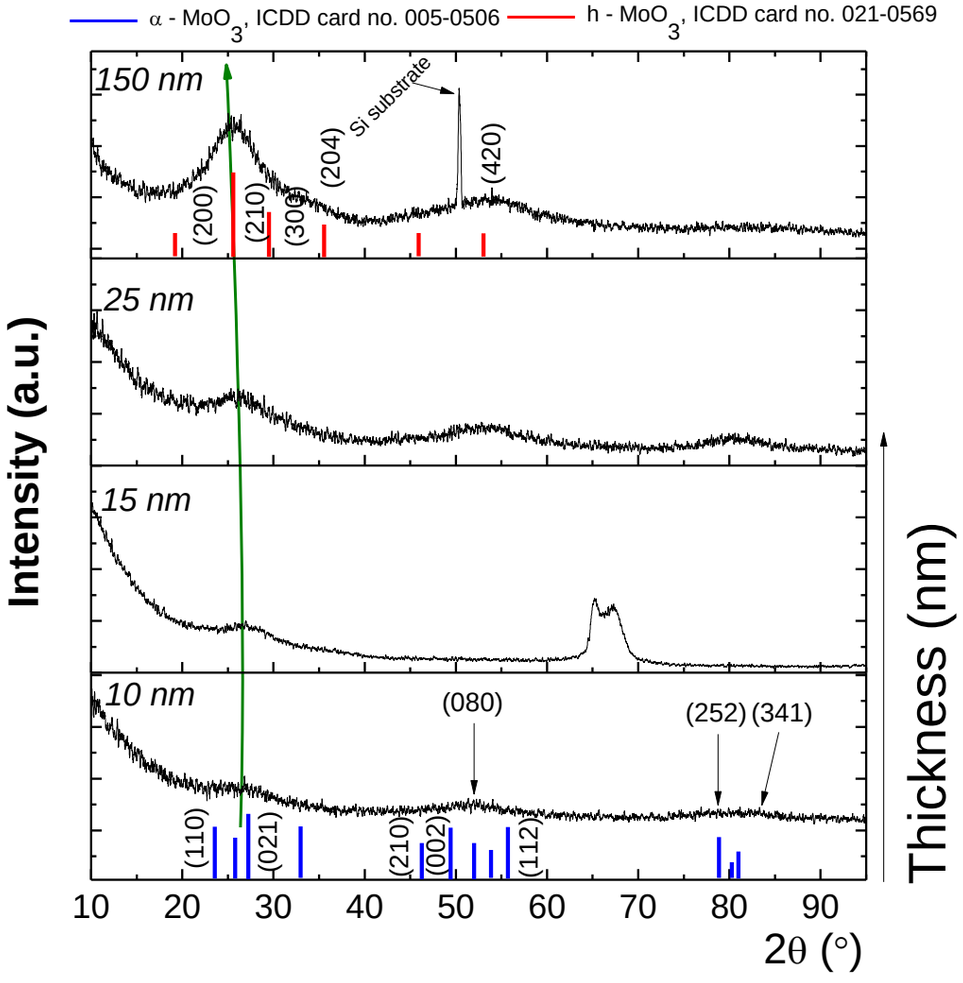


Fig. 3: X-ray diffraction patterns of MoO_3 at different thicknesses. The broad diffraction features were assigned using α- (blue) and h-MoO_3 (red lines) phases.

In each case, the XRD patterns consist of broad diffraction features that indicate the low crystallinity for all these films even at 150 nm. The diffraction features were indexed according to ICDD (International Center of Diffraction Data) database. The blue lines were used to show the theoretical positions of the main α-MoO_3 diffraction peaks, while the red ones for h-MoO_3. At 10 and 15 nm, the first diffraction feature is centered at 27.31° which corresponds to the main reflection of orthorhombic α-MoO_3 phase (ICDD card no. 005-0506) with a = 0.39 nm; b

ACCEPTED MANUSCRIPT
Journal of Applied Physics
AIP Publishing
This is the author's peer reviewed, accepted manuscript. However, the online version of record will be different from this version once it has been copyedited and typeset.
PLEASE CITE THIS ARTICLE AS DOI: 10.1063/5.0151117

= 1.38 nm; c = 0.37 nm with Pbnm(62) spatial group. Further, this diffraction feature is centered at 26.19°, and then this becomes narrower, and at the same time is shifted to 25.78° at 150 nm. The diffraction peak and the right shoulder can be assigned as (210) and (300) reflections of h-MoO_3 (ICDD card no. 021-0569) with a = b = 1.05 nm and c = 1.48 nm. XRD findings suggest that the thickness increasing favour the orthorhombic-hexagonal transition.

UV-VIS-NIR spectrophotometry

The results are shown in Fig. 4 and the transmission spectra are typical for the semiconductor behaviour of $MoO_{2.94}$ [17], with a good optical transmission in the visible range and a decrease in transmission in the NIR spectral range. From the exponential decrease of transmission in the UV range, an estimation for the as-deposited $MoO_{2.94}$ absorption edge was obtained to be around 400±5 nm; therefore, an estimation for the optical bandgap was obtained, i.e., $E_g \approx 3.1$ eV, which is in good agreement with the previously reported data [6, 16]. We should mention that the reduction of the bandgap when compared to that of fully stoichiometric MoO_3 (3.2 eV) is due to the presence of oxygen vacancies in the $MoO_{2.94}$ film and can be also due to the presence of nanocrystalline hexagonal phase of MoO_3 (h-MoO_3) that have been revealed by the XRD measurements.

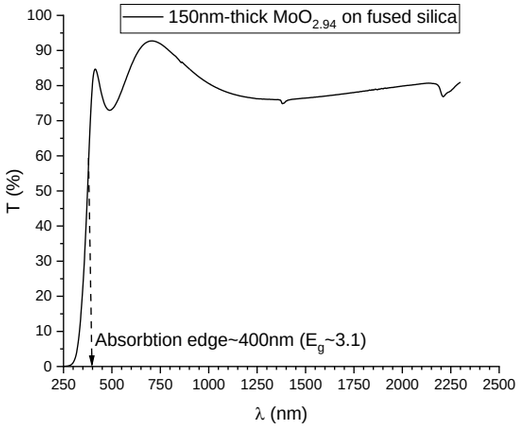
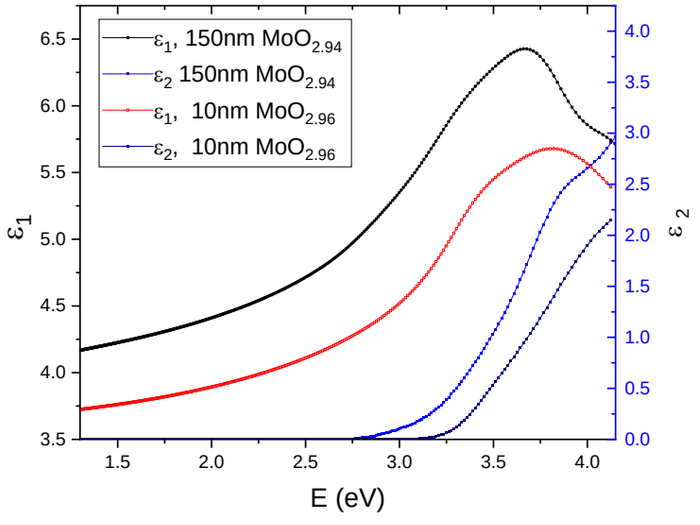


Fig. 4: UV-VIS-NIR optical transmittance for 150nm-thick $MoO_{2.94}$ film deposited on a fused silica substrate. The dotted line intercept indicates the optical absorption edge.

ACCEPTED MANUSCRIPT
Journal of Applied Physics
AIP Publishing
This is the author's peer reviewed, accepted manuscript. However, the online version of record will be different from this version once it has been copyedited and typeset.
PLEASE CITE THIS ARTICLE AS DOI: 10.1063/5.0151117

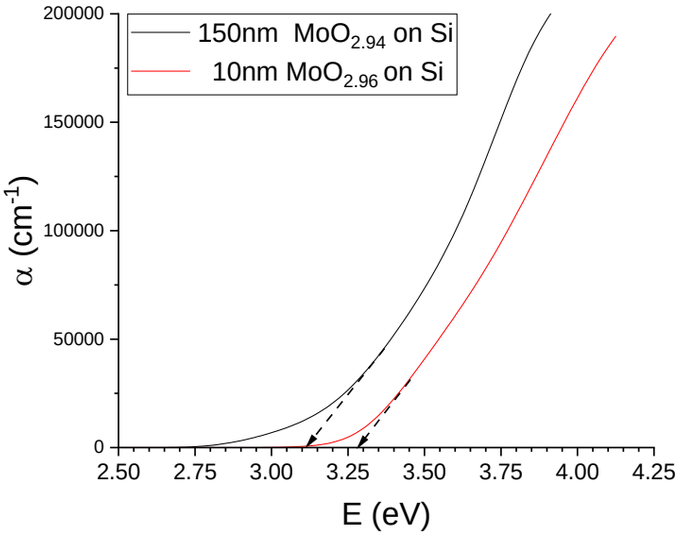
Spectroscopic ellipsometry

The dispersions of the optical constants (real and imaginary part of the dielectric function, ε_1 and ε_2) for as-deposited 150nm-thick $MoO_{2.94}$ and 10nm-thick $MoO_{2.96}$ films is shown in Fig. 5a and these results are found to be in good agreement with the previously reported data [6]. Fig. 5b shows the dispersion of the absorption coefficient α or 150nm-thick $MoO_{2.94}$ and 10nm-thick $MoO_{2.96}$ films. From the onset of the absorption coefficient, an estimation of the optical bandgap was obtained, i.e., 3.10±0.05 eV for $MoO_{2.94}$ (in good agreement with the results estimated from the optical spectrophotometry measurements) and, respectively, 3.26±0.05 eV for 10nm-thick $MoO_{2.96}$. One can notice here that these results indicate the presence of large below-the-bandgap features that are usually associated with the presence of defects like (in our case) the oxygen vacancies revealed by XPS measurements. This is consistent with the presence of a larger sub-bandgap feature for the molybdenum trioxide films with a larger concentration of oxygen vacancies.



(a)

ACCEPTED MANUSCRIPT
Journal of Applied Physics
AIP Publishing
This is the author's peer reviewed, accepted manuscript. However, the online version of record will be different from this version once it has been copyedited and typeset.
PLEASE CITE THIS ARTICLE AS DOI: 10.1063/5.0151117



(b)

Fig. 5: (a) The dispersions of the optical constants (real and imaginary part of the dielectric function, ε_1 and ε_2) for as-deposited 150nm-thick $MoO_{2.94}$ and 10nm-thick $MoO_{2.96}$ films; (b) the dispersions of absorption coefficient α for as-deposited 150nm-thick $MoO_{2.94}$ and 10nm-thick $MoO_{2.96}$ films. The dotted lines intercept indicates the optical bandgap for these films.

4. Electrical characterization and discussion

The electrical characterization of the MoO_{3-x} devices (see Fig. 1) was performed on-wafer and at room temperature employing a Keithley SCS 4200 station. The entire probe station for on-wafer measurements is placed inside a Faraday cage and is connected to the station via low-noise amplifiers. Fitting algorithms were intentionally excluded during or after electrical measurements, and data have been collected on up to 20 devices for each MoO_{3-x} thickness.

First, we measured the thin-film MoO_3-based devices depicted in Fig. 1 and having the thicknesses of 10, 15, and 25 nm deposited on doped Si.

The typical current-voltage (*I*–*V*) dependence of the 10nm-thick $MoO_{2.94}$ devices is depicted in Fig. 6 in the voltage range [-3, 3] V. We observe a typical rectification behaviour of an *n*-

ACCEPTED MANUSCRIPT
Journal of Applied Physics
AIP Publishing
This is the author's peer reviewed, accepted manuscript. However, the online version of record will be different from this version once it has been copyedited and typeset.
PLEASE CITE THIS ARTICLE AS DOI: 10.1063/5.0151117

type semiconductor, which is specific for MoO_3. However, increasing the voltage range we see an abrupt jump in the current value, which was intentionally limited to 10 mA to avoid the breakdown of the devices during measurements.

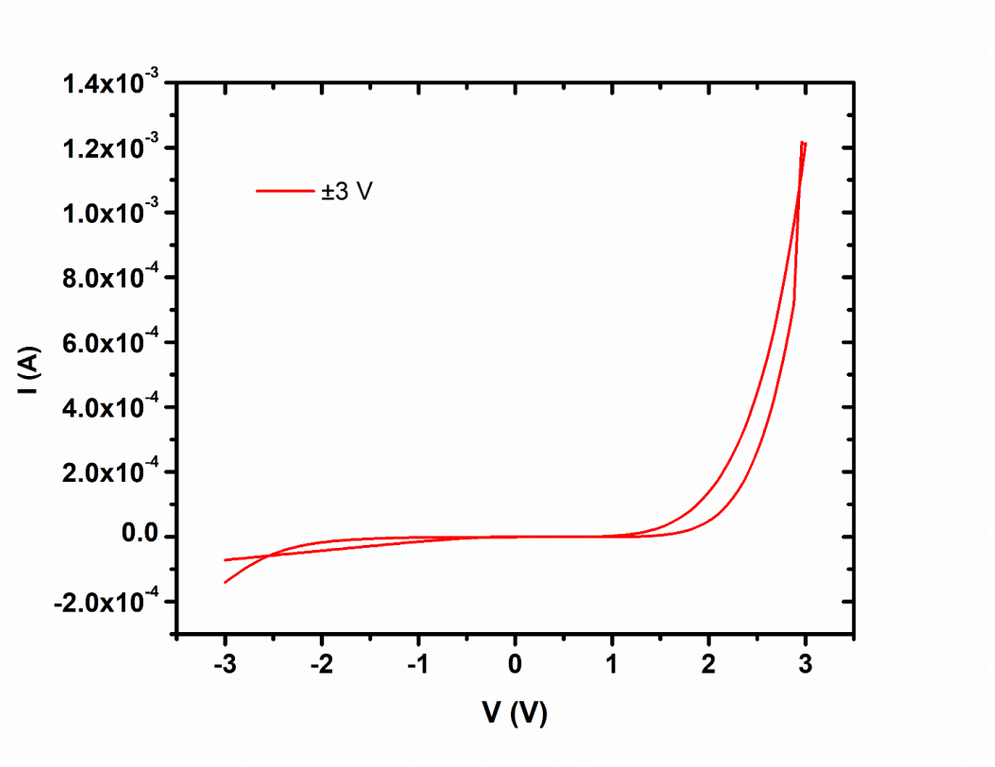


Fig. 6: The typical *I–V* dependence of the 10nm-thick $MoO_{2.94}$-based devices in the voltage range [-3, +3] V.

We have made double-sweep *I–V* measurements, which are depicted in Fig. 7 in the forward and backward directions. We observe that there is a strong reversible phase transition from an insulator state, corresponding to 27.5 MΩ at a voltage value of -9 V, to an average resistance of 80 Ω between +5 and +9 V. The same behavior was noted for tens of devices having a thickness of 10 nm and 15 nm. How can we explain such a strong switching behaviour considering that the threshold of the phase transition is at 3.2 V? There are several explanations in the literature, as follows.

ACCEPTED MANUSCRIPT
Journal of Applied Physics
AIP Publishing
This is the author's peer reviewed, accepted manuscript. However, the online version of record will be different from this version once it has been copyedited and typeset.
PLEASE CITE THIS ARTICLE AS DOI: 10.1063/5.0151117

The first answer is found in Ref. [15]: the phase transition is explained by the change of MoO_3 from an amorphous phase (insulator) to a crystalline phase. However, if we look at the results of Ref. [15] and the supplementary data therein, we observe in the TEM picture the phase change from amorphous to a crystalline state, but further transitions occur among various crystalline phases of MoO_3 since the current never returns to its initial value. These considerations were made for MoO_3 samples having a thickness of 450 nm [15].

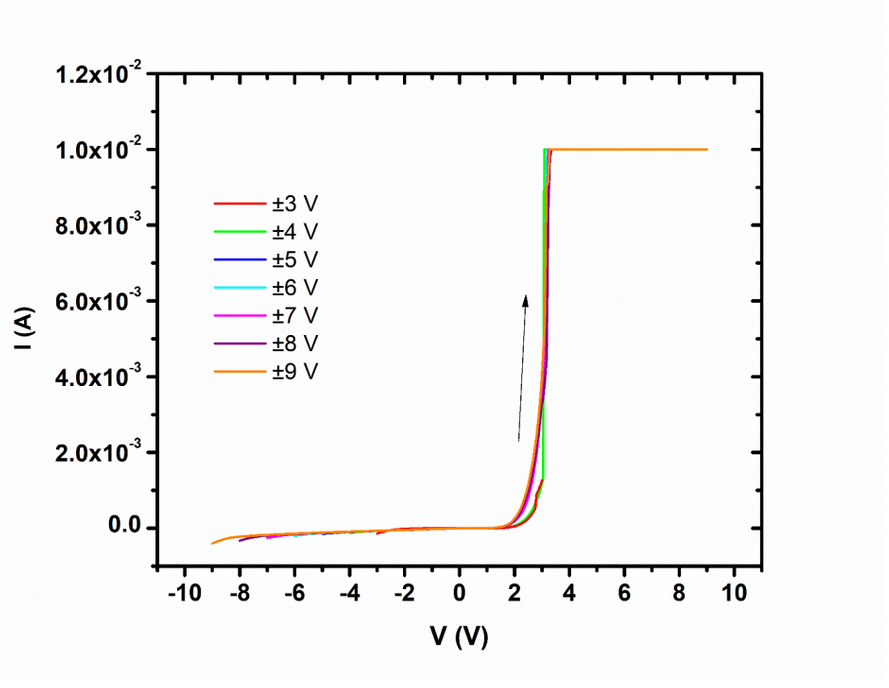
We have selected two $MoO_{2.96}$ samples for TEM measurements, with the nominal thickness of 15 and 25 nm that were measured after the electrical measurements. We have carefully selected an area where we can see the mark left on the top gold contact by the electrical probe, and the cross-section of the TEM images are shown in Fig. 8a and 8b. We can observe from the TEM cross-section that after electrical measurement only a fraction of the $MoO_{2.96}$ has been crystallised. Interestingly, we can notice that this $MoO_{2.96}$ crystalline layer (formed after electric measurement) has the same thickness (9±0.2 nm) for both 15nm-thick and 25nm-thick $MoO_{2.96}$. We are planning as part of our future work to get access to a correction aberration high resolution TEM to repeat these measurements to get even more insights on the microstructural changes that takes places after insulator-to-metal transition.

Therefore, we have looked for an alternative explanation applicable to our case, where the MoO_3 thickness is only 10 nm (for this reason, it is considered as a thin-film MoO_3 in [10]). Atomistic simulations based on DFT calculations have shown that at certain electric field values the lattice of MoO_3 is so much distorted due to the presence of oxygen vacancy. In these cases it was noticed that asymmetric bonding around Mo atoms occurs, Mo-Mo distances are reduced and Mo 3D orbital start overlapping, and the bandgap is closed, so the MoO_{3-x} becomes metallic [17, 19, 20]. Indeed, in Fig. 9 we present the phase transition in $MoO_{2.96}$ thin film (10nm-thick) and we have calculated the subthreshold slope (SS) in a way similar to what is done for FETs, as follows: SS = log(I)/decade and we have obtained 48.3 mV/decade, this value being lower

ACCEPTED MANUSCRIPT
Journal of Applied Physics
AIP Publishing
This is the author's peer reviewed, accepted manuscript. However, the online version of record will be different from this version once it has been copyedited and typeset.
PLEASE CITE THIS ARTICLE AS DOI: 10.1063/5.0151117

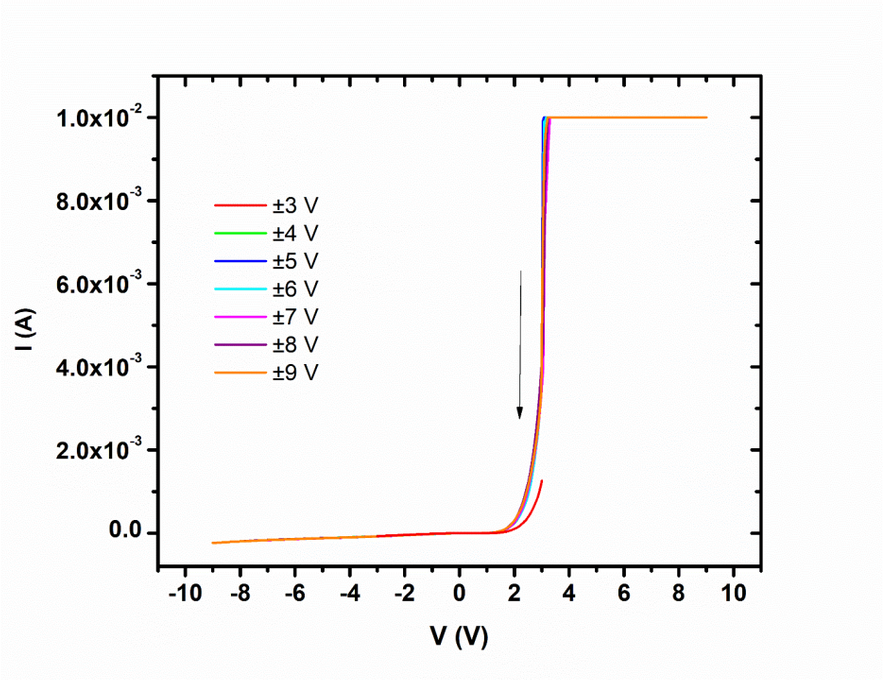
than that in CMOS transistors, and representing a transition from an insulator to a metallic state. The electric field threshold for such transition is found to be equal to 0.23 V/Å [19] (using DFT calculations), while from our experiments it is found to be equal to 0.034 V/Å, these discrepancies originating from the limited number of atoms considered in the DFT calculations.

Hence, we consider that this physical effect occurs in our structures. Also, the phase transitions in MoO_3 were experimentally evidenced in MoO_3 thin films with thicknesses equal to or larger than 100 nm [21, 22]. In the case of MoO_{3-x} thin films with thicknesses of 15 nm and 25 nm, we have found the same phase transitions observed in thinner films. The results are summarized in Table I after 50 cycles of each device. The parameters in the table have shown a remarkable stability since their value is varied with less than 2%.



(a)

ACCEPTED MANUSCRIPT
Journal of Applied Physics
AIP Publishing
This is the author's peer reviewed, accepted manuscript. However, the online version of record will be different from this version once it has been copyedited and typeset.
PLEASE CITE THIS ARTICLE AS DOI: 10.1063/5.0151117



(b)

Fig. 7: The typical *I–V* dependence in the (a) forward and (b) backward direction of the 10nm-thick $MoO_{2.96}$-based devices in various voltage ranges.

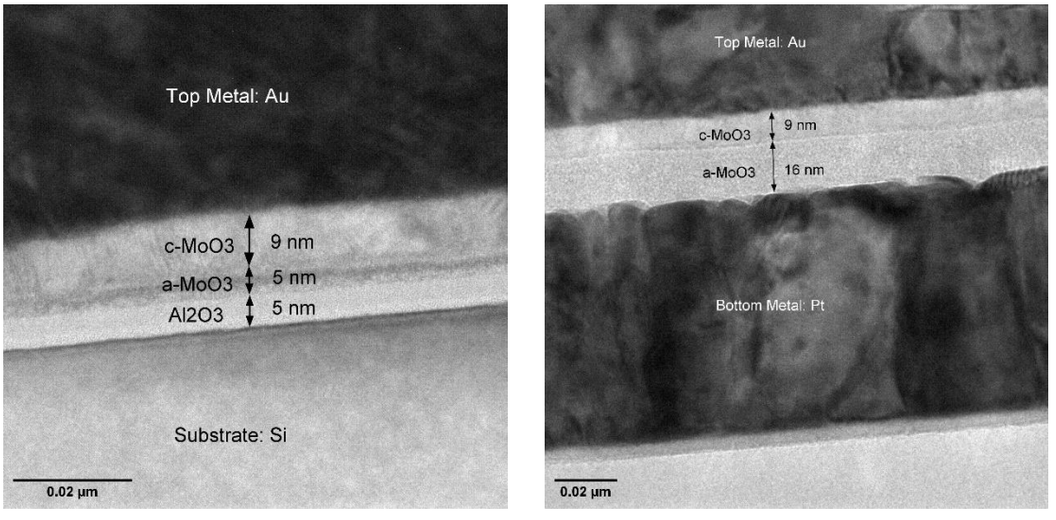


Fig. 8: TEM cross-section done on the two MoO_3-based structures after electrical measurement: 15nm-thick $MoO_{2.96}$ (left picture) and 25nm-thick $MoO_{2.96}$ (right picture).

ACCEPTED MANUSCRIPT
Journal of Applied Physics
AIP Publishing
This is the author's peer reviewed, accepted manuscript. However, the online version of record will be different from this version once it has been copyedited and typeset.
PLEASE CITE THIS ARTICLE AS DOI: 10.1063/5.0151117

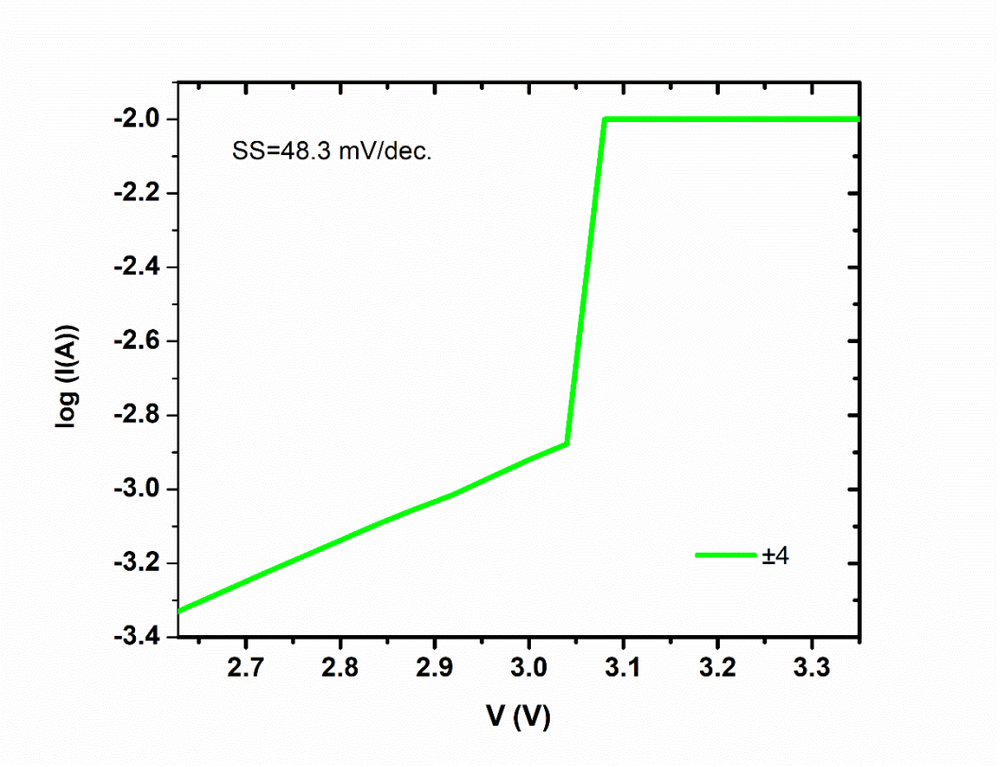


Fig. 9: Subthreshold slope (SS) for the 10nm-thick $MoO_{2.96}$ thin film extracted from the measurement of the current in the voltage range [-4, +4] V.

Table I: Phase transition properties of MoO_3 thin films.

$MoO_{2.96}$ thickness (nm)	Nr. of measured devices	Threshold of phase transition (V)	Hysteresis width (V)
10	18	3	0.1
15	19	5	0.1
25	17	2.5	0.3

Based on these findings we have designed a microwave switch that exploits the abovementioned phase transition. To properly model the switch, we resumed a curve fitting with a Schottky-like model (with an ideality factor much greater than 1, in order to take into

ACCEPTED MANUSCRIPT
Journal of Applied Physics
AIP Publishing
This is the author's peer reviewed, accepted manuscript. However, the online version of record will be different from this version once it has been copyedited and typeset.
PLEASE CITE THIS ARTICLE AS DOI: 10.1063/5.0151117

account the threshold voltage between +1.5 and +2 V). The results are shown in Fig. 10 for the largest interval of values of the applied voltage, i.e., between -9 and +4 V.

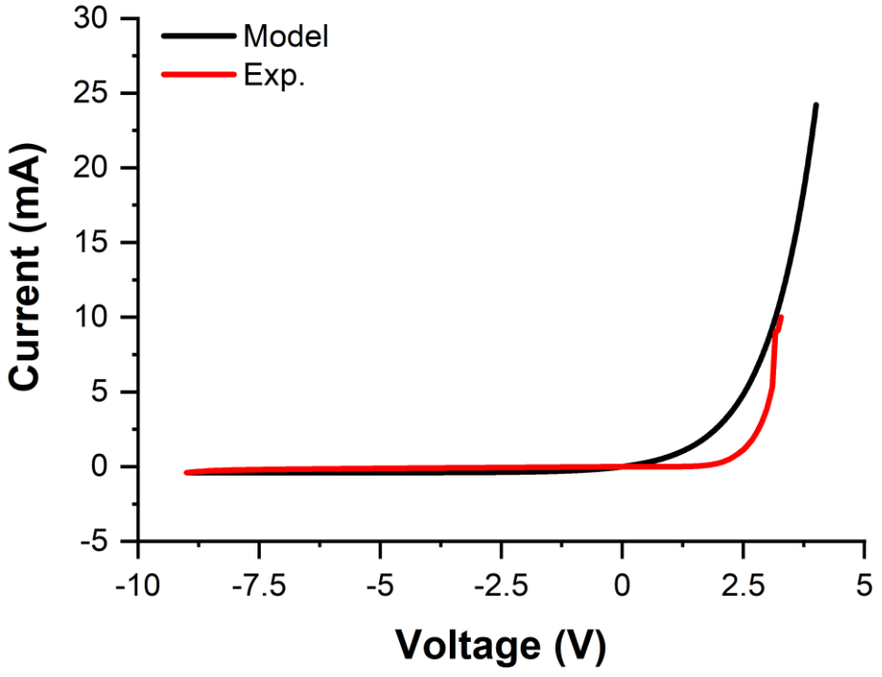


Fig. 10: Circuit modelling of the *I–V* characteristic of the of 10nm-thick MoO_3-based device in the voltage range [-9, +4] V.

From the modelled diode, one can also extract the junction resistance (see Fig. 11), which attains values between 25 MΩ at -9 V and some tens of ohms at 4 V, meaning that we can expect a very good switching behaviour between the off and on states, since the resistance changes with 6 orders of magnitude. Besides this, a junction capacitance of about 10 fF also needs to be modelled, since its effect reflects on the overall shape of the transmission coefficient in the off state.

ACCEPTED MANUSCRIPT
Journal of Applied Physics
AIP Publishing
This is the author's peer reviewed, accepted manuscript. However, the online version of record will be different from this version once it has been copyedited and typeset.
PLEASE CITE THIS ARTICLE AS DOI: 10.1063/5.0151117

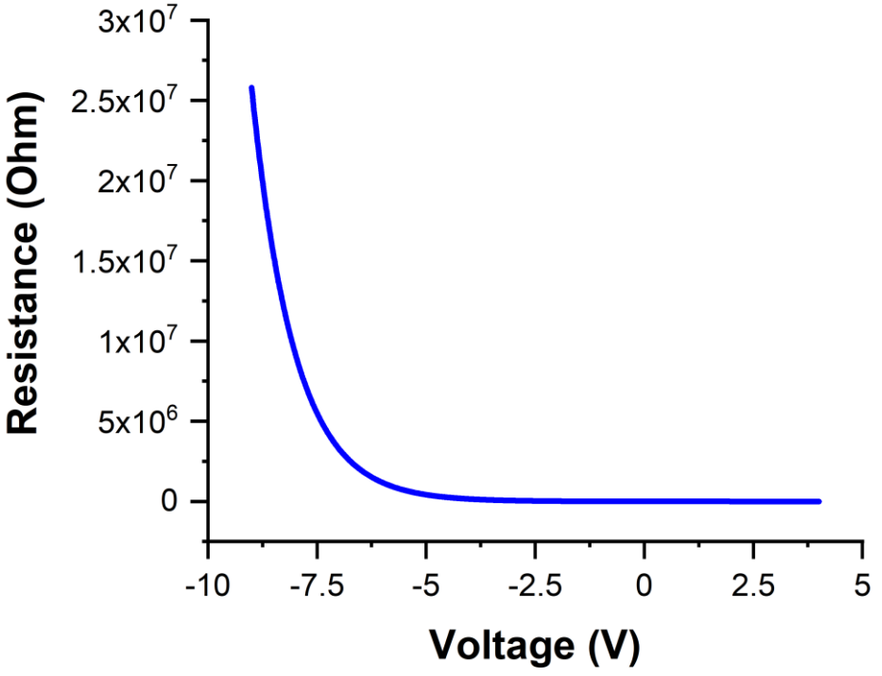
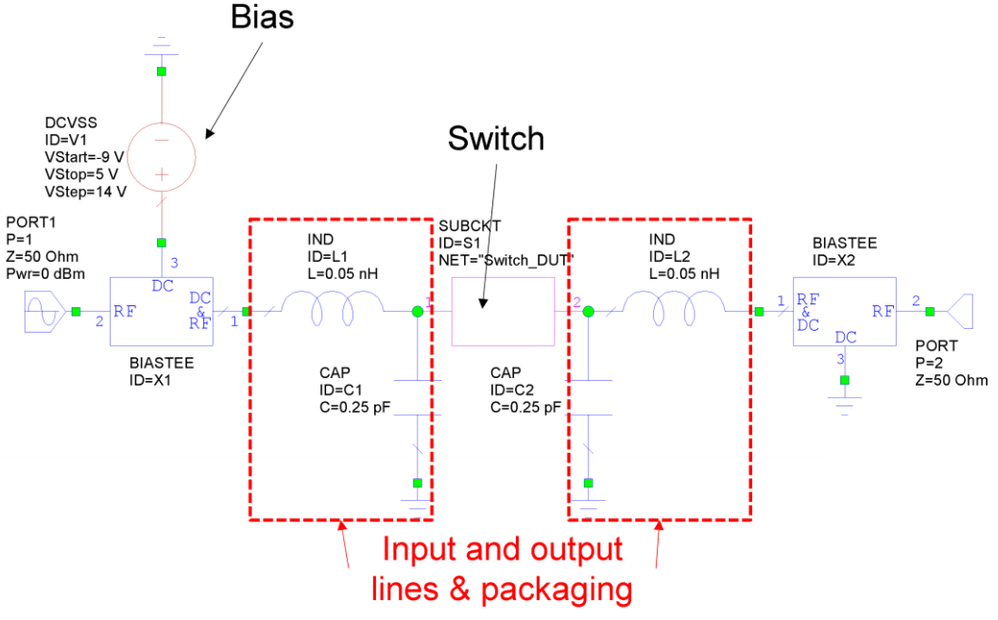


Fig. 11: Resistance of the 10nm-thick MoO_3-based device in the voltage range [-9, +4] V.

The circuit model of the microwave switch is provided in Fig. 12a. The circuit accounts for: (i) an RF input port ("port 1") and an RF output port ("port 2"), both normalized at 50 Ω, with the input port having an adjustable power level (we chose 0 dBm for simplicity); (ii) an input bias tee to provide the proper DC bias to the switch and an output bias tee to short-circuit to ground the output DC signal from the switch, letting only the RF component pass towards the outport port; (iii) input and output lines and packaging (modelled using inductors and capacitors). We chose the frequency range between 0.01 and 10 GHz. The results for the transmission coefficient (from port 1 to port 2) for the off (solid black line) and on (solid red line) states are presented in Fig. 12b. In the off state, the microwave transmission is negligible, whereas in the "on" state it exhibits excellent values between -1.15 dB and -3.02 dB. The obtained results pave the way toward immediate applications in low-power electronics and in atomic-scale microwave switches, which represent a hot research topic [23]. However, there is

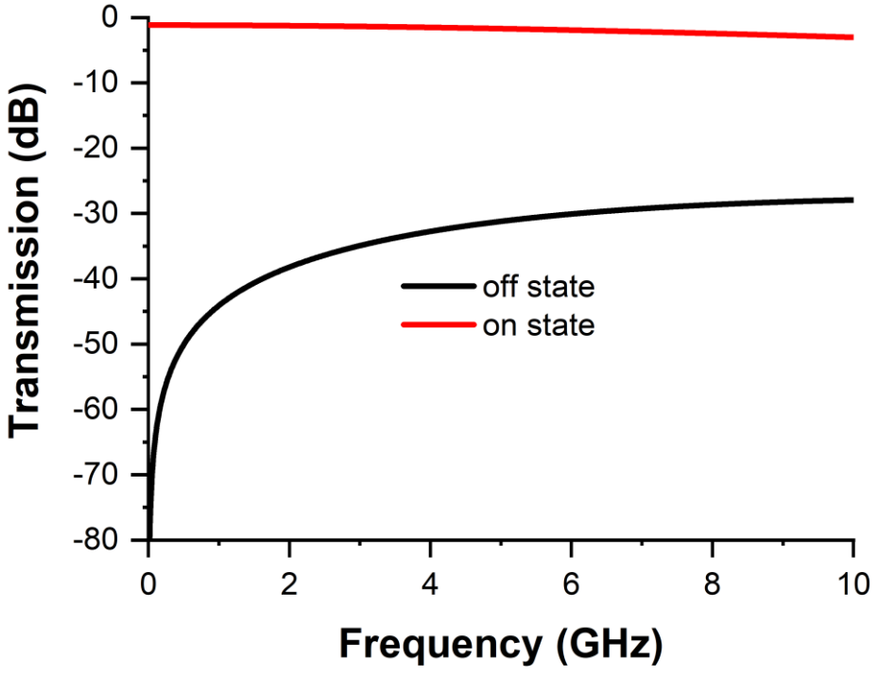
ACCEPTED MANUSCRIPT
Journal of Applied Physics
AIP Publishing
This is the author's peer reviewed, accepted manuscript. However, the online version of record will be different from this version once it has been copyedited and typeset.
PLEASE CITE THIS ARTICLE AS DOI: 10.1063/5.0151117

still much to learn about the underlying mechanisms of this transition, as well as its dependence on film thickness, temperature, and other factors. Future research will investigate these aspects in more detail to better understand the potential of thin-film MoO_3 for practical applications. Another interesting route is the integration of thin-film MoO_3 with other materials and systems to create new devices and applications. Just to give an example, thin-film MoO_3 could be integrated with other two-dimensional (2D) materials, such as graphene or TMDs, to create new heterostructures with ground-breaking electronic and optical properties. Alternatively, MoO_3 could be used as a gate dielectric in FETs or other electronic devices, taking advantage of its low subthreshold slope and IMT behavior.



(a)

ACCEPTED MANUSCRIPT
Journal of Applied Physics
AIP Publishing
This is the author's peer reviewed, accepted manuscript. However, the online version of record will be different from this version once it has been copyedited and typeset.
PLEASE CITE THIS ARTICLE AS DOI: 10.1063/5.0151117



(b)

Fig. 12: (a) Circuit model of the MoO_3-based microwave switch; (b) transmission coefficient (from port 1 to port 2) for the off (solid black line) and on (solid red line) states in the frequency range 0.01-10 GHz.

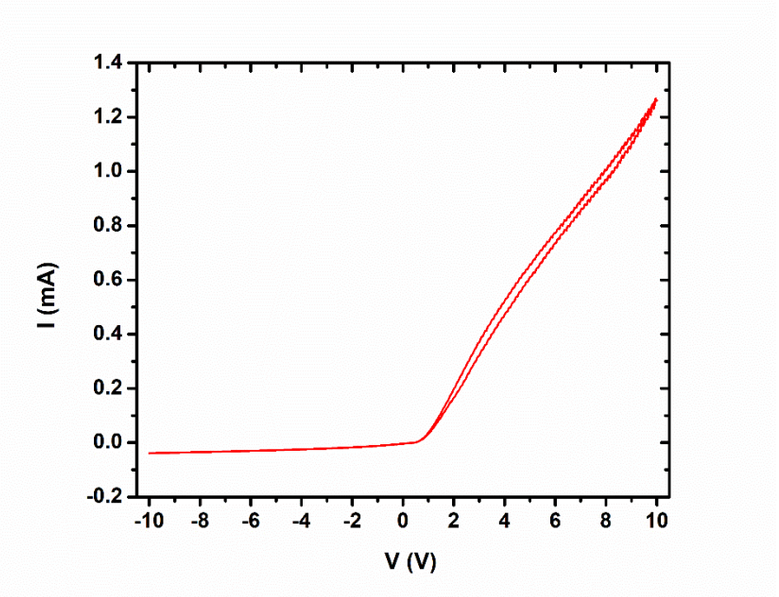
The samples of $MoO_{2.94}$ with a thickness of 150 nm showed no phase transition, the current-voltage characteristics being typical for a semiconductor as depicted in Fig. 13a. We have extended the search for an eventual transition in the voltage range [-20, +20] V but no transition was observed. The presence of oxygen vacancies in our samples drove us to study the ferroelectricity in all samples, since we have recently shown that in NiO thin films the oxygen vacancies break the centrosymmetric nature of the material and, thus, ferroelectricity is produced [24]. The polarization-voltage (*P*–*E*) hysteresis loops were measured using a Sawyer-Tower circuit configuration formed by a digital oscilloscope (Wavesurfer 3024—Teledyne LeCroy) and a pulse generator (NI PXIe-1078—National Instruments). Prior to the MoO_3

ACCEPTED MANUSCRIPT
Journal of Applied Physics
AIP Publishing
This is the author's peer reviewed, accepted manuscript. However, the online version of record will be different from this version once it has been copyedited and typeset.
PLEASE CITE THIS ARTICLE AS DOI: 10.1063/5.0151117

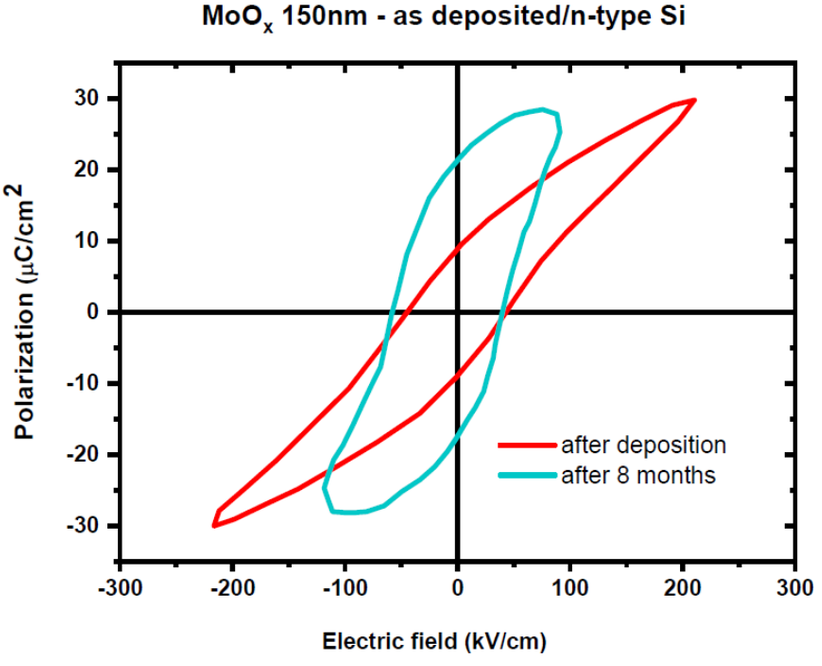
samples, we calibrated the measurement setup with a standard ferroelectric capacitor from Radiant Technologies. The thin-film $MoO_{2.96}$ samples with thicknesses of 10 nm, 15 nm, and 25 nm showed no ferroelectricity. However, the MoO_3 samples with a thickness of 150 nm have shown ferroelectricity manifested by a hysteretic P(E), with a coercive field of about 50 kV/cm, a saturation polarization of about 30 $\mu C/cm^2$, and a remanent polarization of about 10 $\mu C/cm^2$. The results are presented in Fig. 13b (which is composed of 120 cycles superimposed). After the first *P–E* measurements, we preserved the samples in ambient conditions for 8 months. Then, we thermally treated the samples for 5 min at 300°C in a vacuum to refresh the distribution of oxygen vacancies. The result is presented in Fig. 12b, in which we can see that the coercive field and the saturation polarization are practically unchanged, whereas the remanent polarization is enhanced to a value of about 20 $\mu C/cm^2$.

As we have mentioned from XRD results, the crystalline structure of thicker $MoO_{2.96}$ is different from that of $MoO_{2.94}$ thin films and we have observed the presence of a nanocrystalline hexagonal phase of MoO_3, namely h-MoO_3 that is a metastable phase for MoO_3. We are considering here that the nanocrystalline h-MoO_3 (absent in the $MoO_{2.96}$ thin films) is responsible for the onset of ferroelectricity reported here for the first time. We are also noting here that the presence of oxygen vacancies or the hexagonal phase in the nanocrystalline h-MoO_3 may also play a role in the explanation of ferroelectricity as they distorrt the lattice of h-MoO_3. We have to point out that the oxygen vacancies are responsible for ferroelectricity also in amorphous Al_2O_3 [25], in ZrO_2 thin films [26], or the $SrTiO_3/SrRuO_3$ superlattices [27].

ACCEPTED MANUSCRIPT
Journal of Applied Physics
AIP Publishing
This is the author's peer reviewed, accepted manuscript. However, the online version of record will be different from this version once it has been copyedited and typeset.
PLEASE CITE THIS ARTICLE AS DOI: 10.1063/5.0151117



(a)



(b)

Fig. 13: (a) *I–V* characteristic of the 150nm-thick MoO_3-based device in the voltage range [-10, +10] V; (b) (*P–E*) hysteresis loops of the 150nm-thick $MoO_{2.94}$ thin film after deposition (solid red line) and after 8 months (solid blue line).

ACCEPTED MANUSCRIPT
Journal of Applied Physics
AIP Publishing
This is the author's peer reviewed, accepted manuscript. However, the online version of record will be different from this version once it has been copyedited and typeset.
PLEASE CITE THIS ARTICLE AS DOI: 10.1063/5.0151117

Conclusions

In this work, we have presented the experimental evidence of the reversible insulator-metal transitions in MoO_3 thin films having immediate applications in low-power electronics thanks to a SS lower than 60 mV/dec at 3 V, and in atomic-scale microwave switches that represent a hot research topic. Such a strong switching behaviour, considering that the threshold of the phase transition is at 3.2 V, can be explained in a twofold manner: (i) the phase transition is induced by the change of MoO_3 from an amorphous phase (insulator) to a crystalline phase (applicable for 450nm-thick MoO_3 films); (ii) for MoO_3 thin films with a thickness of only 10 nm (the present case of study), the phase transition is induced by an external electric field, which distorts so much the lattice of MoO_3 due to the migration of the oxygen vacancies that the bandgap closes and the MoO_3 becomes metallic. This leads to a SS of just 48.3 mV/decade, which is the proof of a transition from an insulator to a metallic state. We have also proposed the design of a microwave switch that exploits the abovementioned phase transition: in the frequency range 0.01-10 GHz, the transmission coefficient exhibits excellent values between -1.15 dB and -3.02 dB in “on” state, while in “off “state it is practically negligible. Finally, thicker samples of MoO_3 (150 nm) show ferroelectricity, thus adding MoO_3 to the list of materials with a ferroelectric behaviour induced by oxygen vacancies. The discovered ferroelectric phase is also very stable in time and under ambient exposure, with practically constant values for both coercive field and saturation polarization, and a doubled value for the remanent polarization after a short high-temperature thermal treatment aimed at refreshing the distribution of oxygen vacancies.

Acknowledgments

ACCEPTED MANUSCRIPT
Journal of Applied Physics
AIP Publishing
This is the author's peer reviewed, accepted manuscript. However, the online version of record will be different from this version once it has been copyedited and typeset.
PLEASE CITE THIS ARTICLE AS DOI: 10.1063/5.0151117

This research was partially funded by the European Commission under the Grant No. 951761 'NANO-EH', and by the Romanian Ministry of Research, Innovation and Digitalization, CCCDI—UEFISCDI, under Project PN-III-P4-PCE-2021-0223, Project PN-III-P3-3.6-H2020-2020-0072, and Project PN-III-P2-2.1-PED-2021-3183, within PNCDI III. The XPS measurements were caried out under the contract PN 23.21.01.06 sponsored by the Romanian Ministry of Research, Innovation and Digitalization.

Data Availability Statement

The data that support the findings of this study are available from the corresponding author upon reasonable request.

References

1N. F. Mott, Rev. Mod. Phys. 40, 677 (1968).

2H. Wang, H. Yuan, S. S. Hong, Y. Lib, and Y. Cui, Chem. Soc. Rev. 44, 2664, (2015).

3G. Álvarez-Pérez, T. G. Folland, I. Errea, J. Taboada-Gutiérrez, J. Duan, J. Martín-Sánchez, A. I. F. Tresguerres-Mata, J. R. Matson, A. Bylinkin, M. He, W. Ma, Q. Bao, J. I. Martín, J. D. Caldwell, A. Y. Nikitin, and P. Alonso-González, Adv. Mater. 32, 1908176 (2020).

4M. Chen, X. Lin, T. H. Dinh, Z Zheng, J. Shen, Q. Ma, H. Chen, P. Jarillo-Herrero, and S. Dai, Nat. Mater. 19, 1307 (2020).

5Q. Zhang, X. Li, Q. Ma, Q. Zhang, H. Bai, W. Yi, J. Liu, J. Han, and G. Xi, Nat. Commun. 8, 14903 (2017).

6Y. Gutiérrez, G. Santos, F. Palumbo, M. Modreanu, F. Moreno, and M. Losurdo, Opt. Mater. Express 12, 3957 (2022).

7I. Alves de Castro, R. S. Datta, J. Z. Ou, A. Castellanos-Gomez, S. Sriram, T. Daeneke, and K. Kalantar-zadeh, Adv. Mater. 29, 1701619 (2017).

ACCEPTED MANUSCRIPT
Journal of Applied Physics
AIP Publishing
This is the author's peer reviewed, accepted manuscript. However, the online version of record will be different from this version once it has been copyedited and typeset.
PLEASE CITE THIS ARTICLE AS DOI: 10.1063/5.0151117

8X. Hu, K. Liu, Y. Cai, S.-Q. Zang, and T. Zhai, Small 2, 2200008 (2022).

9S. K. Radha, K. Crowley, B. A. Holler, X. P. A. Gao, W. R. L. Lambrecht, H. Volkova, M.-H. Berger, E. Pentzer, K. G. Pachuta, and A. Sehirlioglu, J. Appl. Phys. 129, 220903 (2021).

10S. Balendhran, S. Walia, H. Nili, J. Z. Ou, S. Zhuiykov, R. B. Kaner, S. Sriram, M. Bhaskaran, and K. Kalantar-zadeh, Adv. Funct. Mater. 23, 3952 (2013).

11S. Balendhran, J. Deng, J. Z. Ou, S. Walia, J. Scott, J. Tang, K. L. Wang, M. R. Field, S. Russo, S. Zhuiykov, M. S. Strano, N. Medhekar, S. Sriram, M. Bhaskaran, and K. Kalantar-zadeh, Adv. Mater. 25, 109 (2013).

12M. M. Y. A. Alsaif, A. F. Chrimes, T. Daeneke, S. Balendhran, D. O. Bellisario, Y. Son, M. R. Field, W. Zhang, H. Nili, E. P. Nguyen, K. Latham, J. van Embden, M. S. Strano, J. Z. Ou, and K. Kalantar-zadeh, Adv. Funct. Mater. 26, 91 (2016).

13S. Li, M. Tian, Q. Gao, M. Wang, T. Li, Q. Hu, X. Li, and Y. Wu, Nat. Mater. 18, 1091 (2019).

14Q. Hu, S. Zhu, C. Gu, and Y. Wu, Appl. Phys. Lett. 121, 242101 (2022).

15Y. Ogawa, S. Shindo, Y. Sutou, and J. Koike, Appl. Phys. Lett. 111, 163105 (2017).

16J. Meyer, M. Kröger, S. Hamwi, F. Gnam, T. Riedl, W. Kowalsky, and A. Kahn, Appl. Phys. Lett. 96, 193302 (2010).

17K. Inzani, M. Nematollahi, F. Vullum-Bruer, T. Grande, T. W. Reenaas, and S. M. Selbach, Phys. Chem. Chem. Phys. 19, 9232 (2017).

18F. G. Bell and L. Ley, Phys. Rev. B Condens. Matter. 37, 8383 (1988).

19H. A. Qayyum, M. F. Al-Kuhaili, and T. Hussain, J. Alloys Compd. 921, 16606315 (2022).

20P.-R. Huang, Y. He, C. Cao, and Z.-H. Lu, Sci. Rep. 4, 7131 (2014).

21A. L. Pergament, V. P. Malinenko, L. A. Aleshina, E. L. Kazakova, and N. A. Kuldin, J. Exp. Phys. 2014, 951297 (2014).

22M. Arita, H. Kaji, T. Fujii, and Y. Takahashi, Thin Solid Films 520, 4762 (2012).

ACCEPTED MANUSCRIPT
Journal of Applied Physics
AIP Publishing
This is the author's peer reviewed, accepted manuscript. However, the online version of record will be different from this version once it has been copyedited and typeset.
PLEASE CITE THIS ARTICLE AS DOI: 10.1063/5.0151117

23M. Dragoman, M. Aldrigo, and D. Dragoman, Nanomaterials 11, 625 (2021).

24M. Dragoman, S. Vulpe, E. Aperathithis, C. Aivalioti, C. Romanitan, A. Dinescu, D. Dragoman, M. Aldrigo, N. Djourelov, M. Modreanu, and A. Moldovan, J. Appl. Phys. 131, 164304 (2022).

25Y. Peng, G. Han, F. Liu, W. Xiao, Y. Liu, N. Zhong, C. Duan, Z. Feng, H. Dong, and Y. Hao, Nanoscale Res. Lett. 15, 134 (2020).

26V. Lenzi, J. P. B. Silva, B. Šmíd, V. Matolín, C. M. Istrate, C. Ghica, J. L. MacManus-Driscoll, and L. Marques, Energy & Environmental Materials, First published: 17 August 2022, https://doi.org/10.1002/eem2.12500.

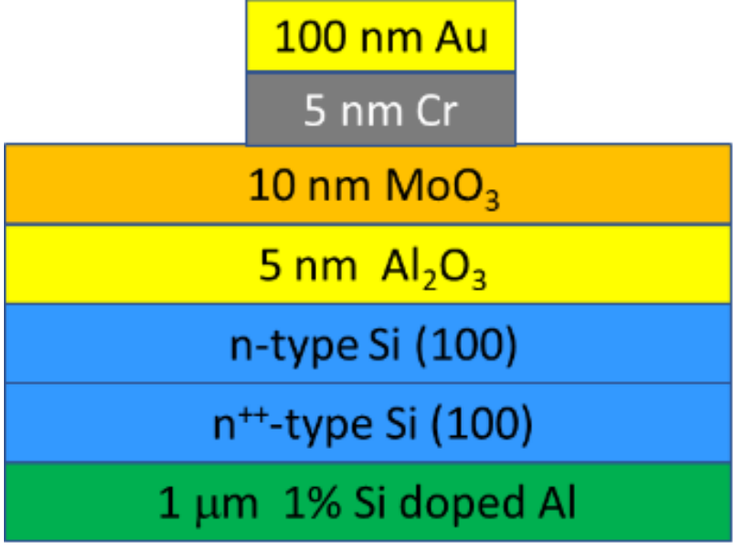
27J. L. Lin, Y. Sun, R. He, Y. Li, Z. Zhong, P. Gao, X. Zhao, Z. Zhang, and Z. J. Wang, Nano Lett. 22, 7104 (2022).

ACCEPTED MANUSCRIPT

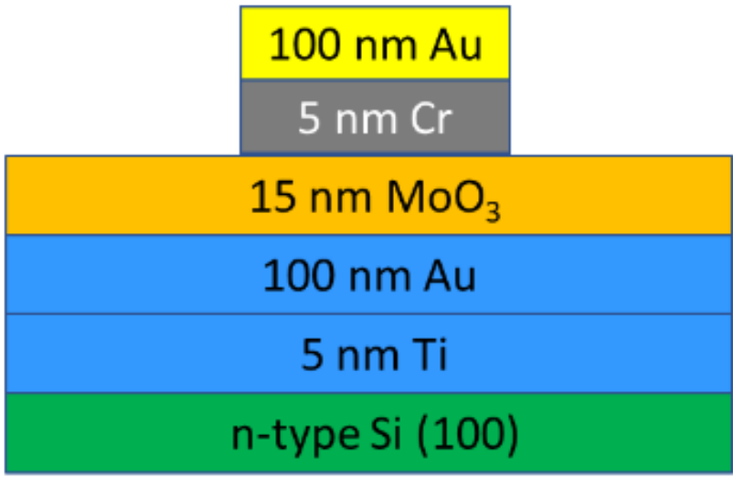
Journal of Applied Physics

AIP Publishing

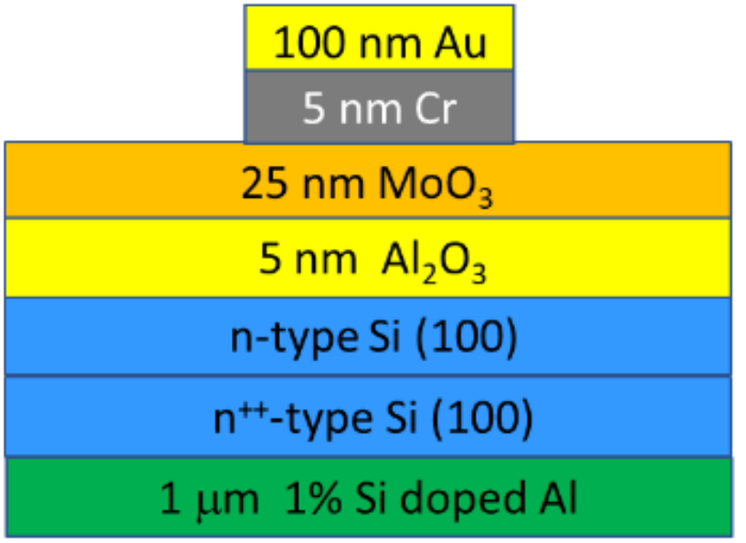
This is the author's peer reviewed, accepted manuscript. However, the online version of record will be different from this version once it has been copyedited and typeset.
PLEASE CITE THIS ARTICLE AS DOI: 10.1063/5.0151117



a



b



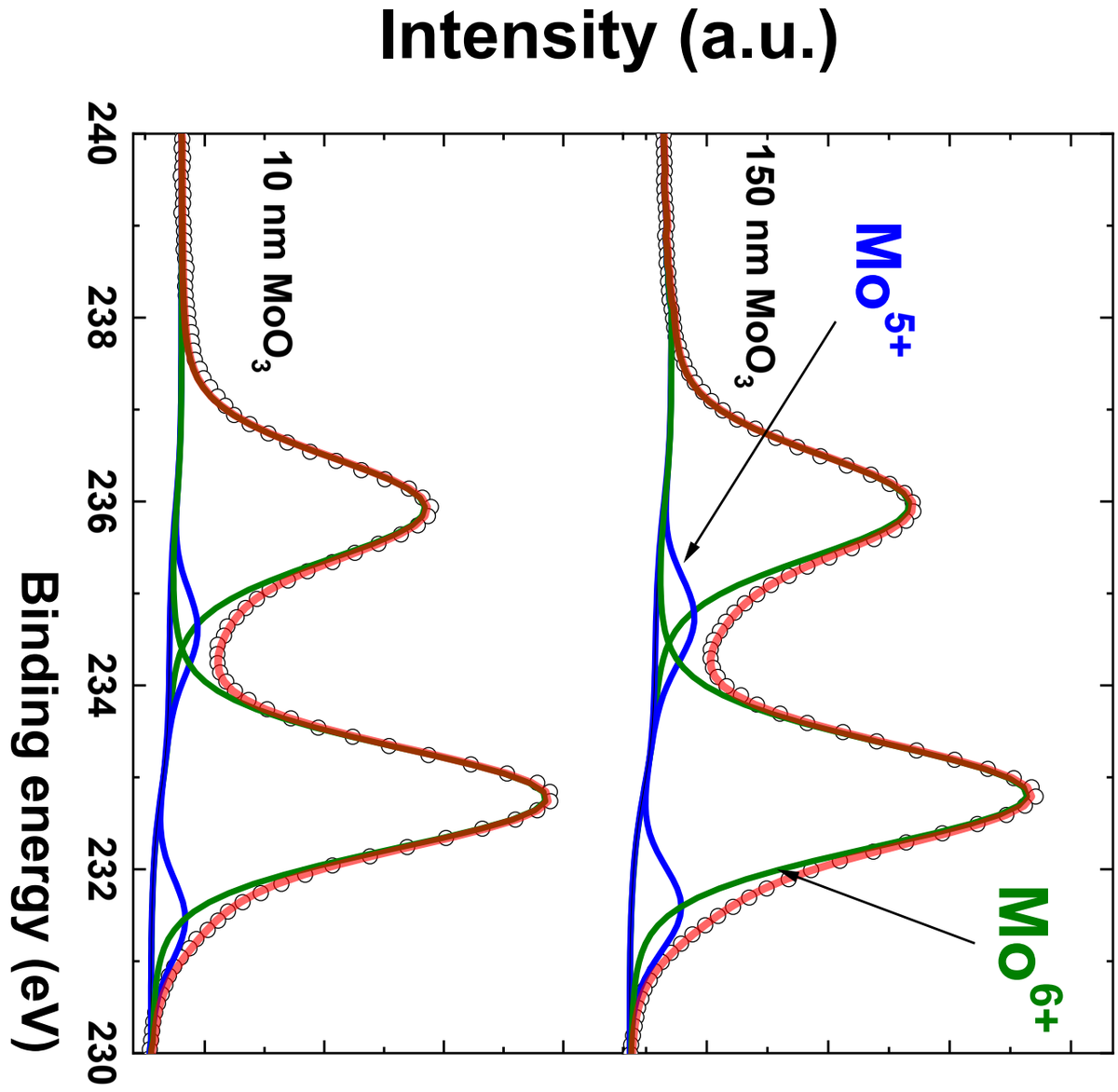
c

AIP Publishing

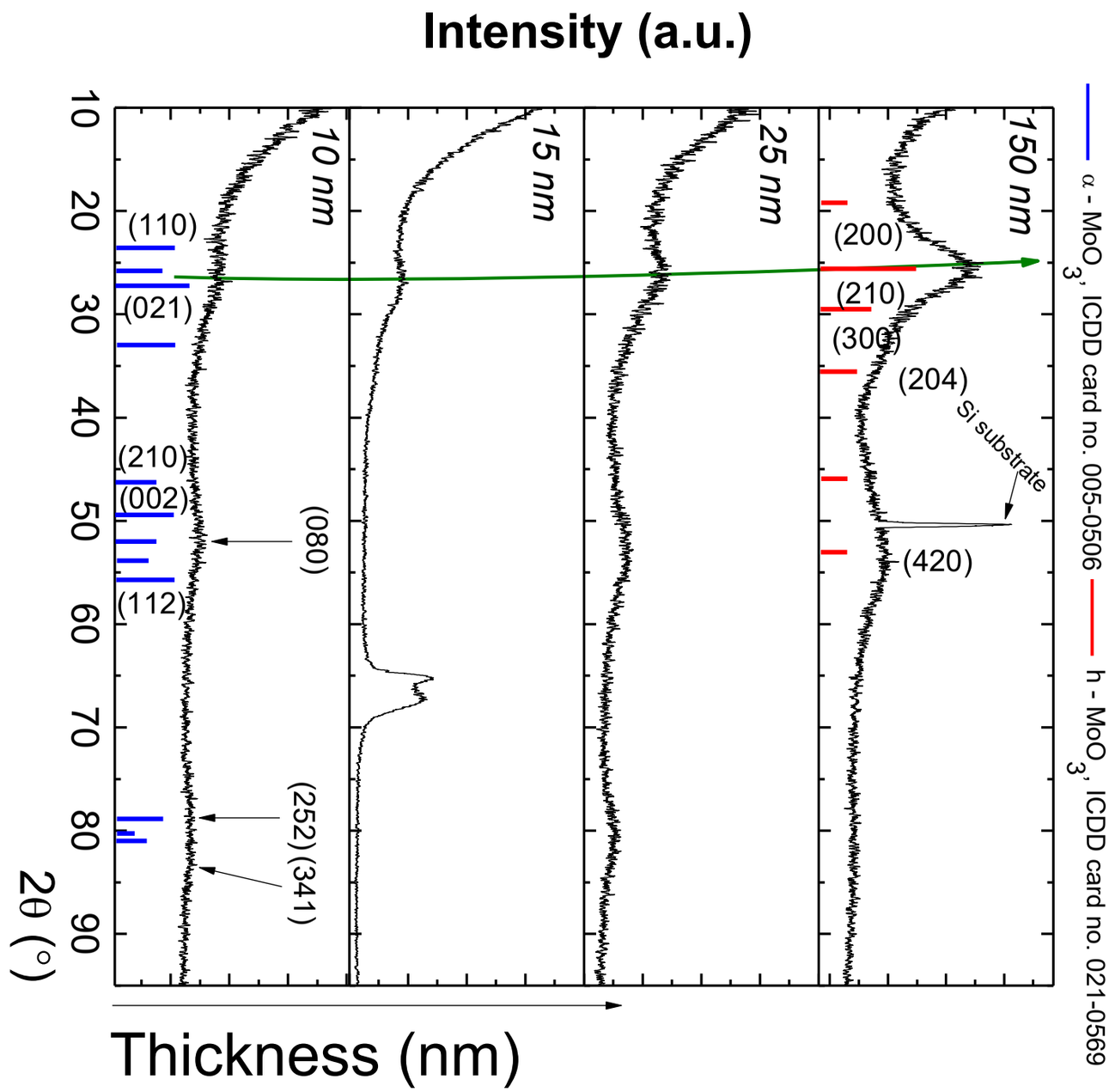
Journal of Applied Physics

ACCEPTED MANUSCRIPT

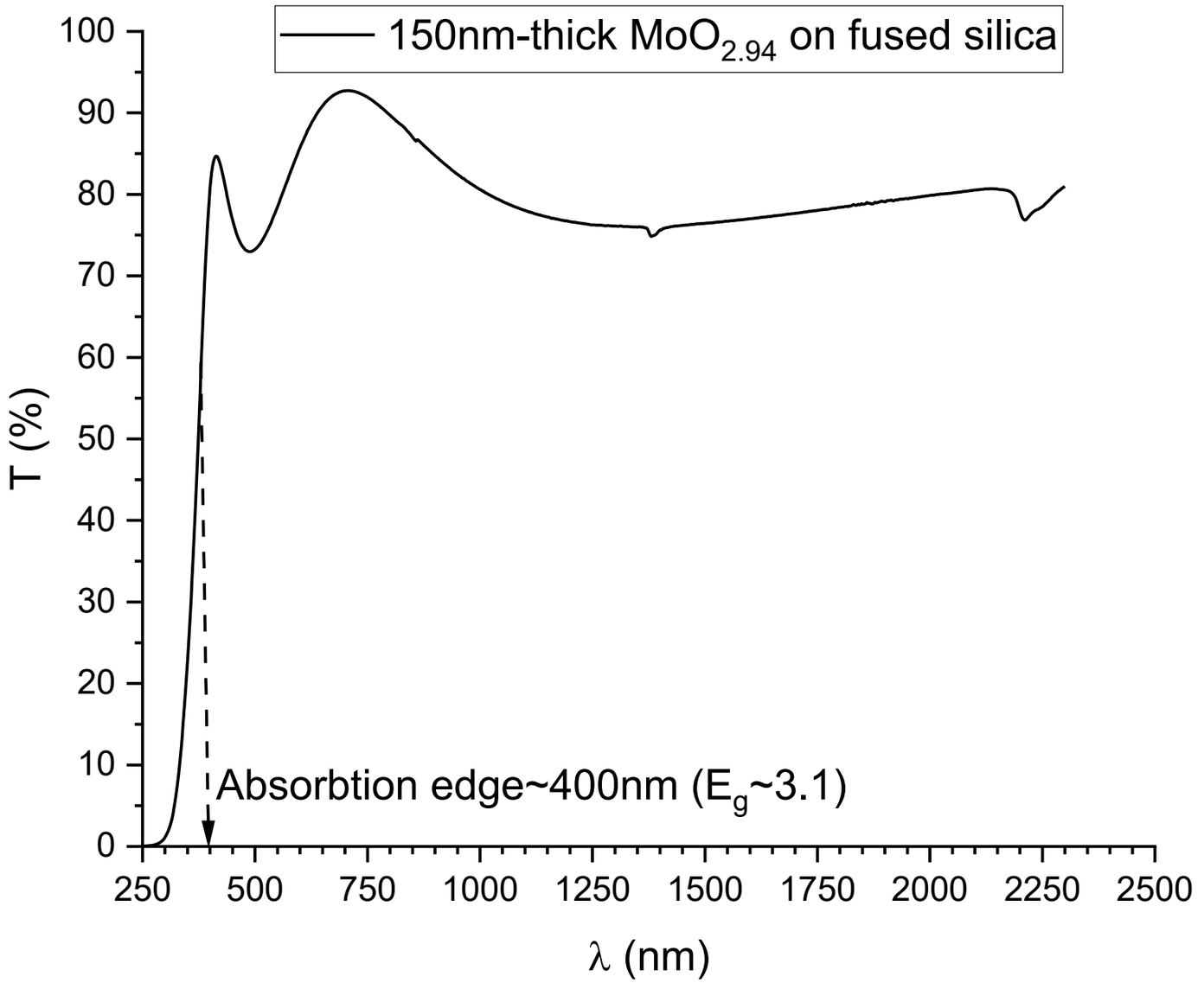
This is the author's peer reviewed, accepted manuscript. However, the online version of record will be different from this version once it has been copyedited and typeset.
PLEASE CITE THIS ARTICLE AS DOI: 10.1063/5.0151117



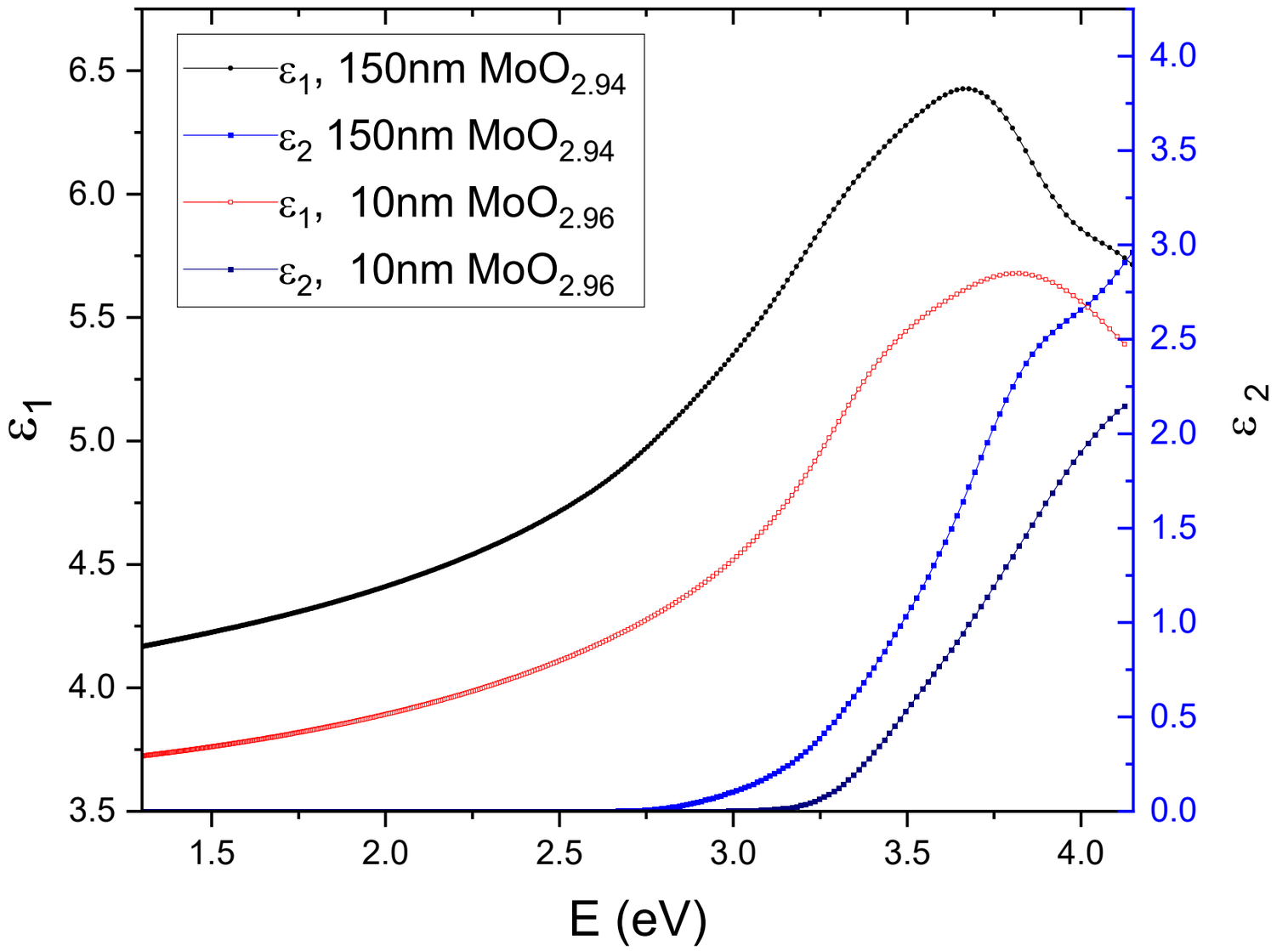
AIP Publishing
Journal of Applied Physics
ACCEPTED MANUSCRIPT
This is the author's peer reviewed, accepted manuscript. However, the online version of record will be different from this version once it has been copyedited and typeset.
PLEASE CITE THIS ARTICLE AS DOI: 10.1063/5.0151117



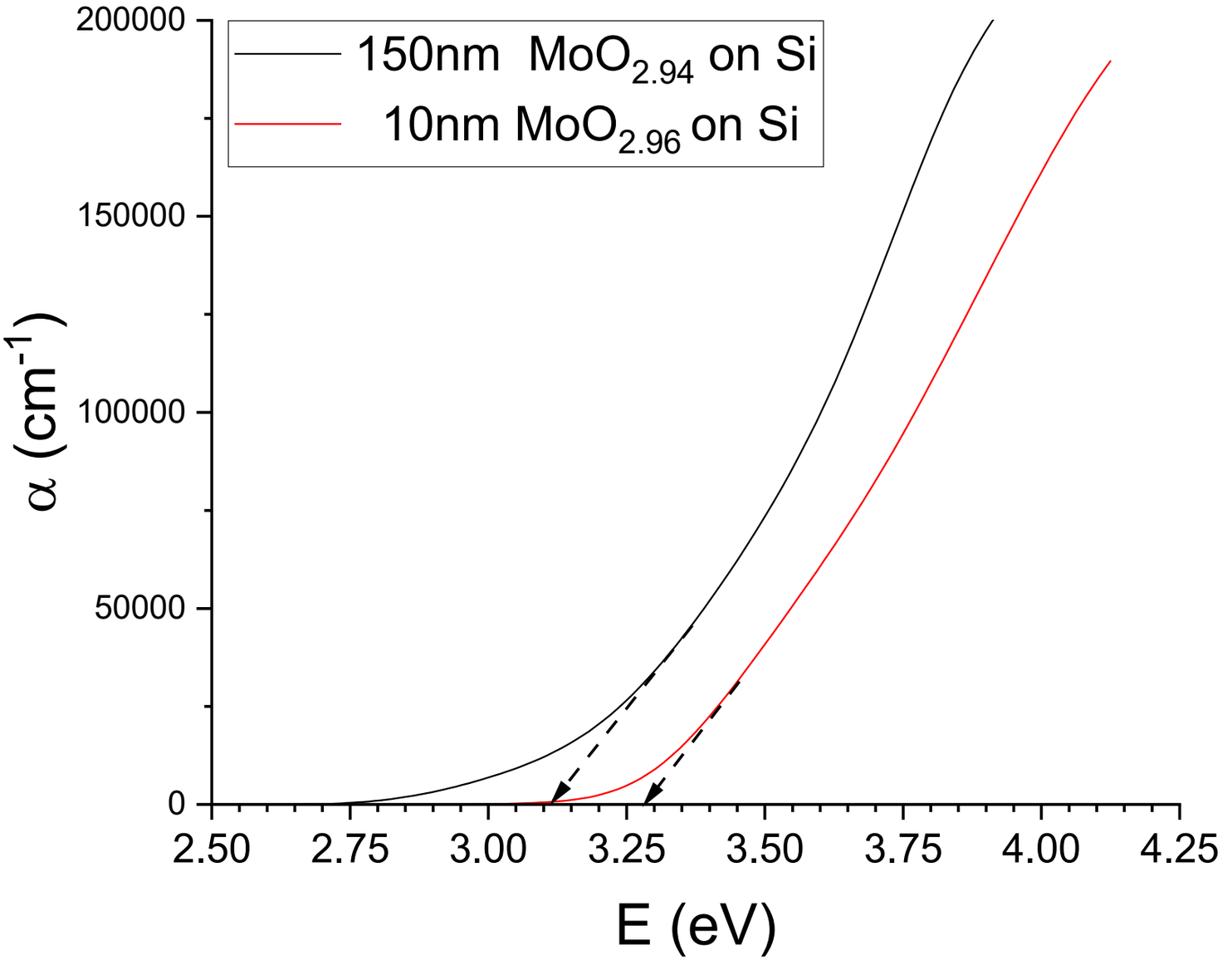
ACCEPTED MANUSCRIPT
Journal of Applied Physics
AIP Publishing
This is the author's peer reviewed, accepted manuscript. However, the online version of record will be different from this version once it has been copyedited and typeset.
PLEASE CITE THIS ARTICLE AS DOI: 10.1063/5.0151117



ACCEPTED MANUSCRIPT
Journal of Applied Physics
AIP Publishing
This is the author's peer reviewed, accepted manuscript. However, the online version of record will be different from this version once it has been copyedited and typeset.
PLEASE CITE THIS ARTICLE AS DOI: 10.1063/5.0151117



ACCEPTED MANUSCRIPT
Journal of Applied Physics
AIP Publishing
This is the author's peer reviewed, accepted manuscript. However, the online version of record will be different from this version once it has been copyedited and typeset.
PLEASE CITE THIS ARTICLE AS DOI: 10.1063/5.0151117

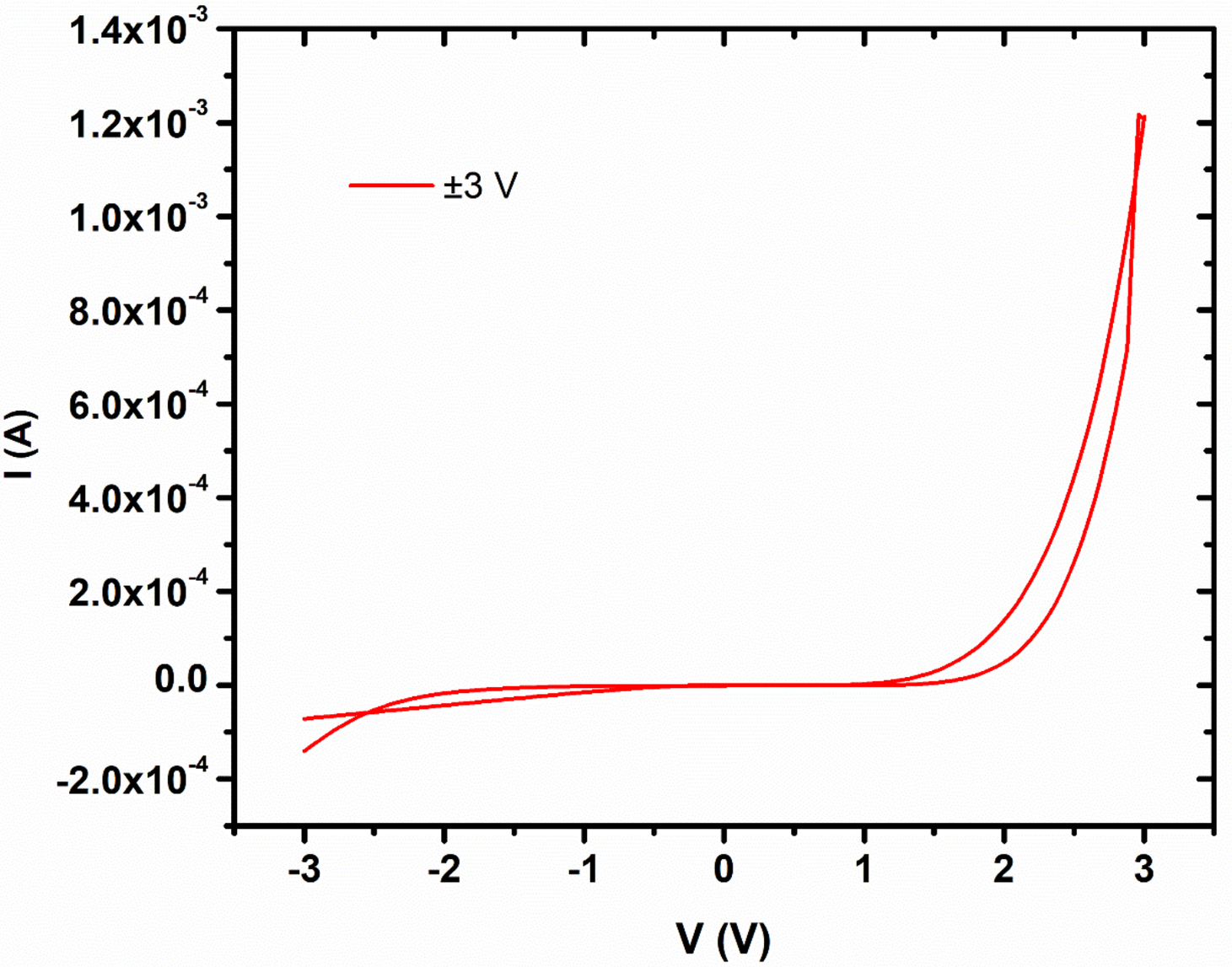


ACCEPTED MANUSCRIPT

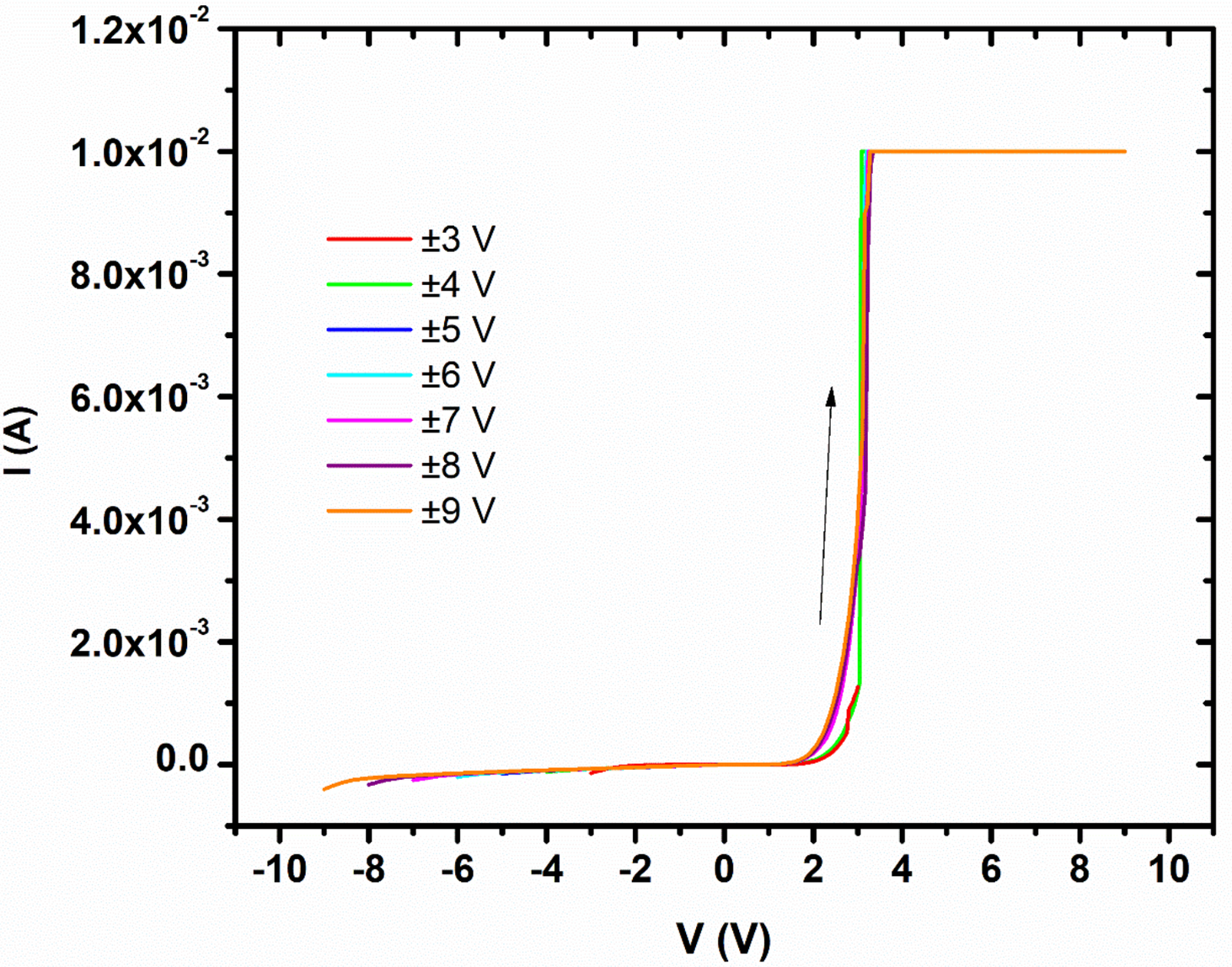
Journal of Applied Physics

AIP Publishing

This is the author's peer reviewed, accepted manuscript. However, the online version of record will be different from this version once it has been copyedited and typeset.
PLEASE CITE THIS ARTICLE AS DOI: 10.1063/5.0151117



ACCEPTED MANUSCRIPT
Journal of Applied Physics
AIP Publishing
This is the author's peer reviewed, accepted manuscript. However, the online version of record will be different from this version once it has been copyedited and typeset.
PLEASE CITE THIS ARTICLE AS DOI: 10.1063/5.0151117

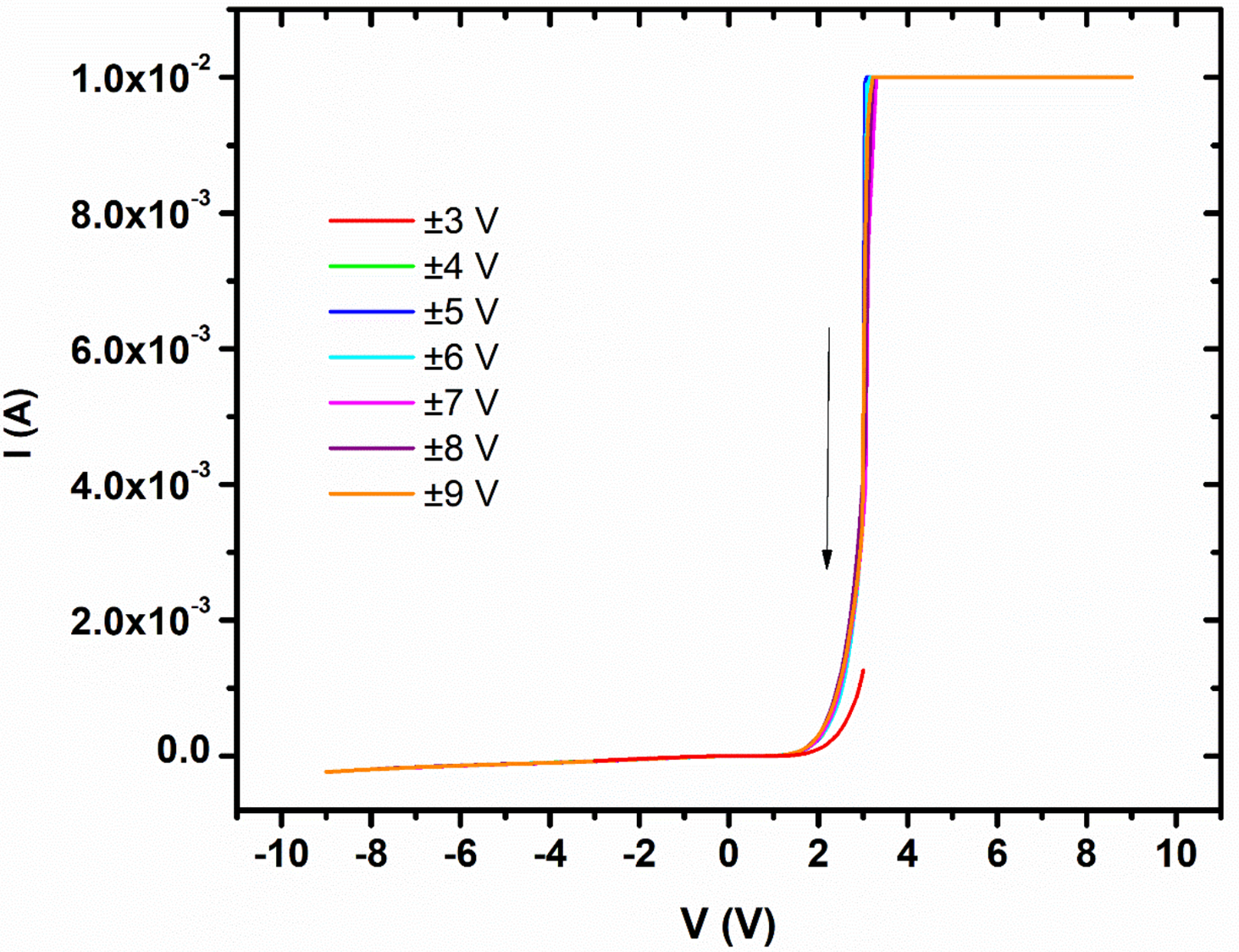


ACCEPTED MANUSCRIPT

Journal of Applied Physics

AIP Publishing

This is the author's peer reviewed, accepted manuscript. However, the online version of record will be different from this version once it has been copyedited and typeset.
PLEASE CITE THIS ARTICLE AS DOI: 10.1063/5.0151117



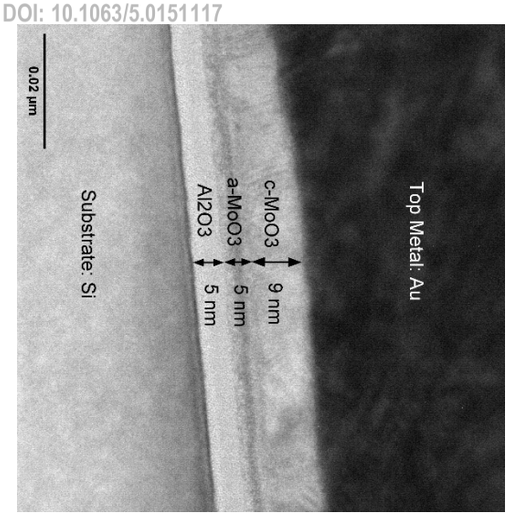
AIP Publishing

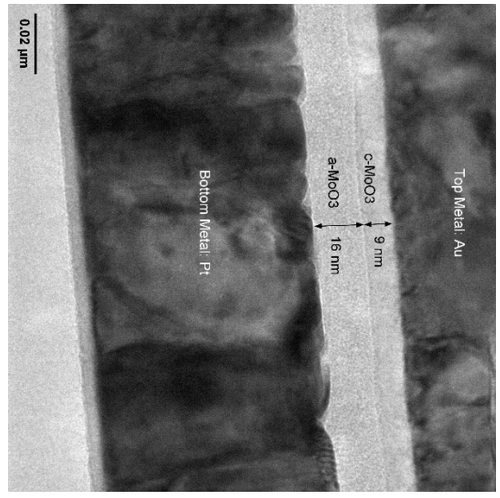
Journal of Applied Physics

ACCEPTED MANUSCRIPT

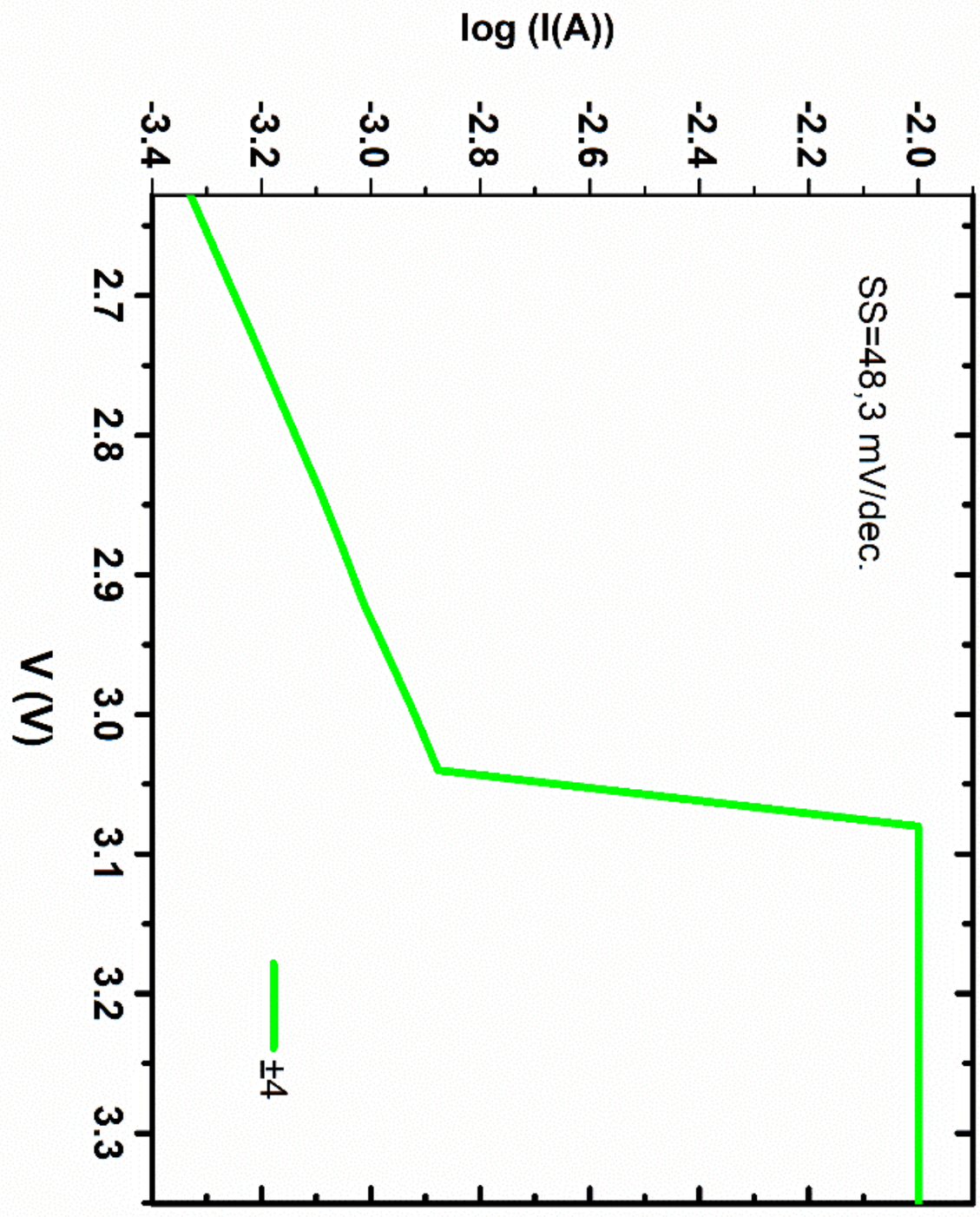
This is the author's peer reviewed, accepted manuscript. However, the online version of record will be different from this version once it has been copyedited and typeset.

PLEASE CITE THIS ARTICLE AS DOI: 10.1063/5.0151117

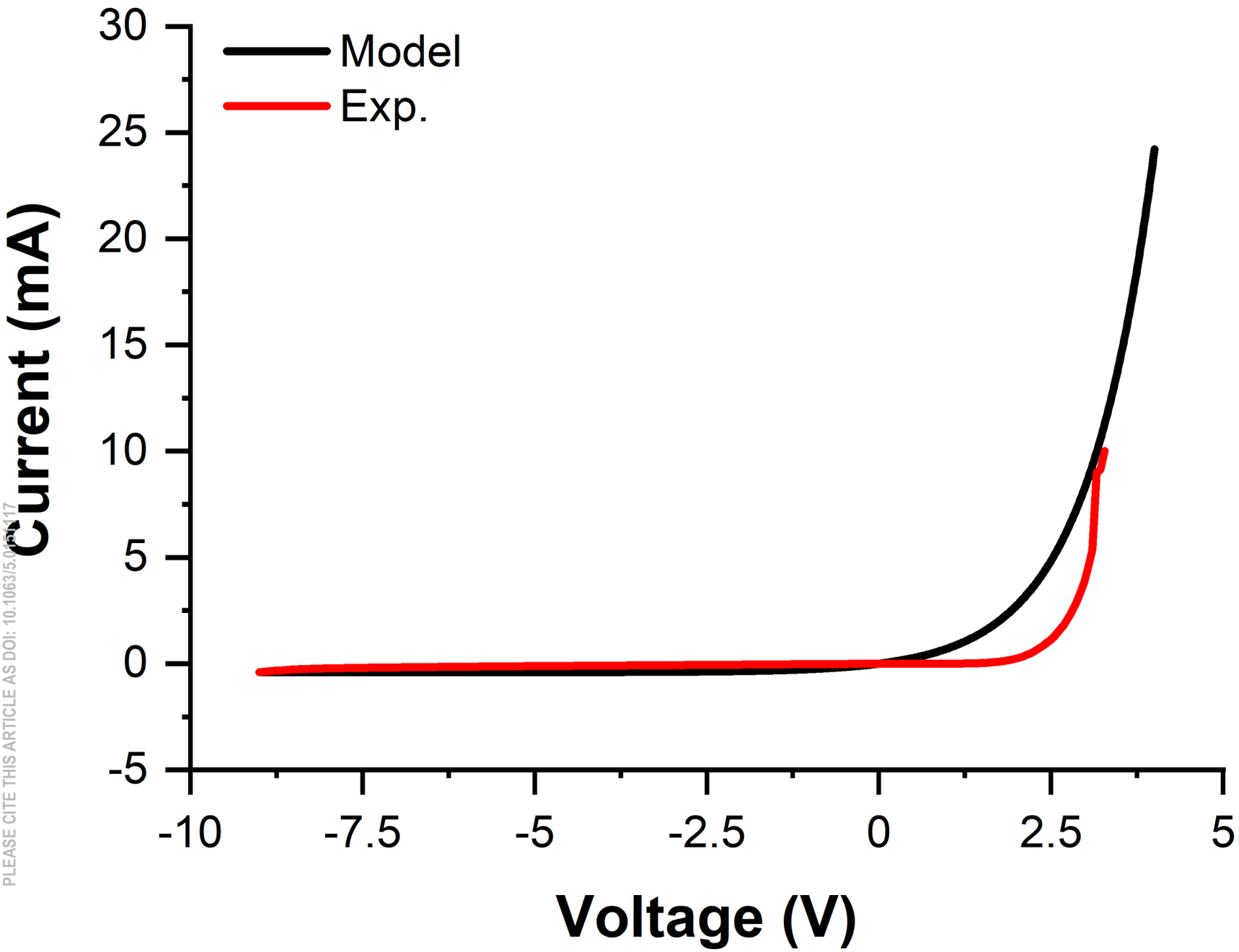




AIP Publishing
Journal of Applied Physics
ACCEPTED MANUSCRIPT
This is the author's peer reviewed, accepted manuscript. However, the online version of record will be different from this version once it has been copyedited and typeset.
PLEASE CITE THIS ARTICLE AS DOI: 10.1063/5.0151117



ACCEPTED MANUSCRIPT
Journal of Applied Physics
AIP Publishing
This is the author's peer reviewed, accepted manuscript. However, the online version of record will be different from this version once it has been copyedited and typeset.
PLEASE CITE THIS ARTICLE AS DOI: 10.1063/5.0057117

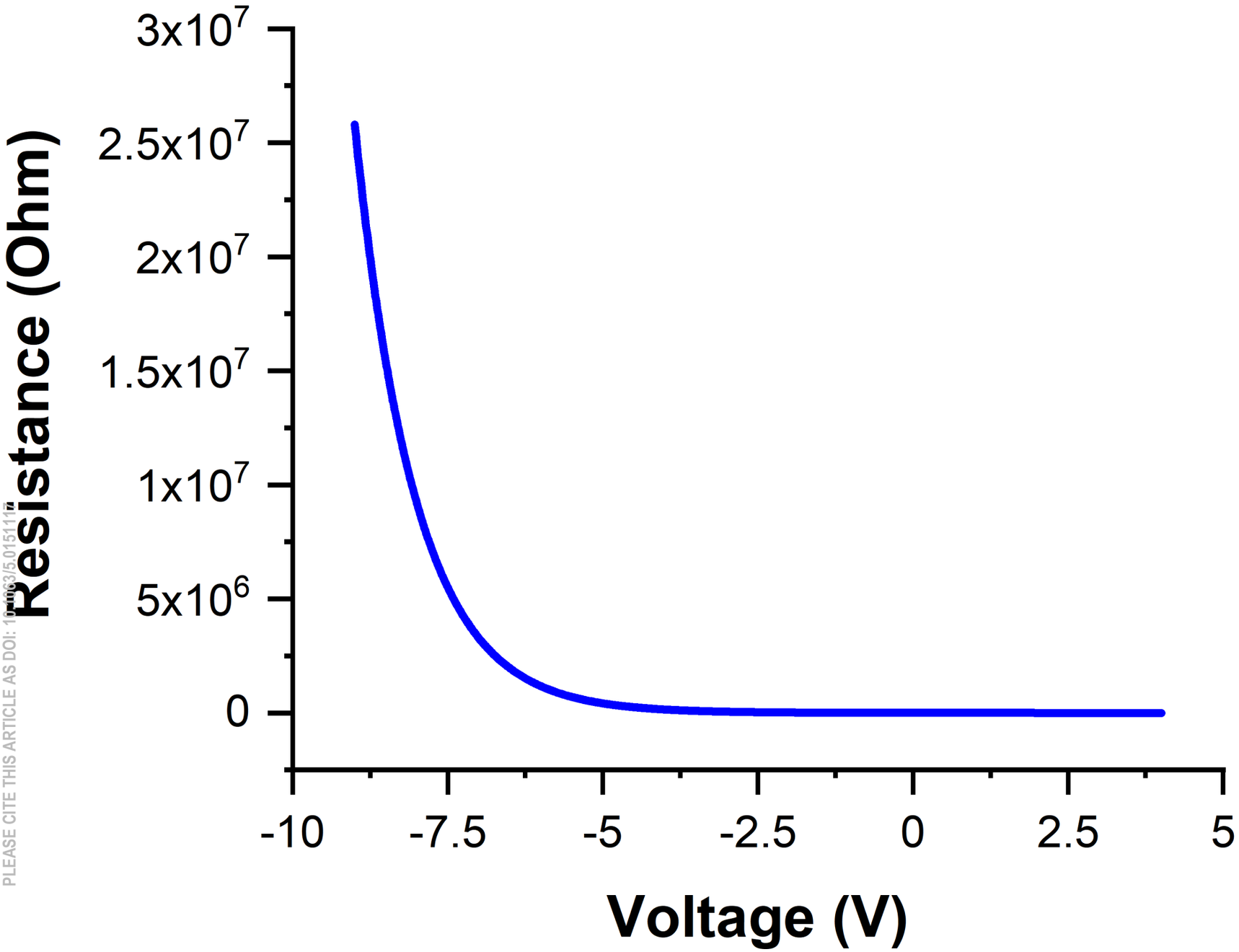


ACCEPTED MANUSCRIPT

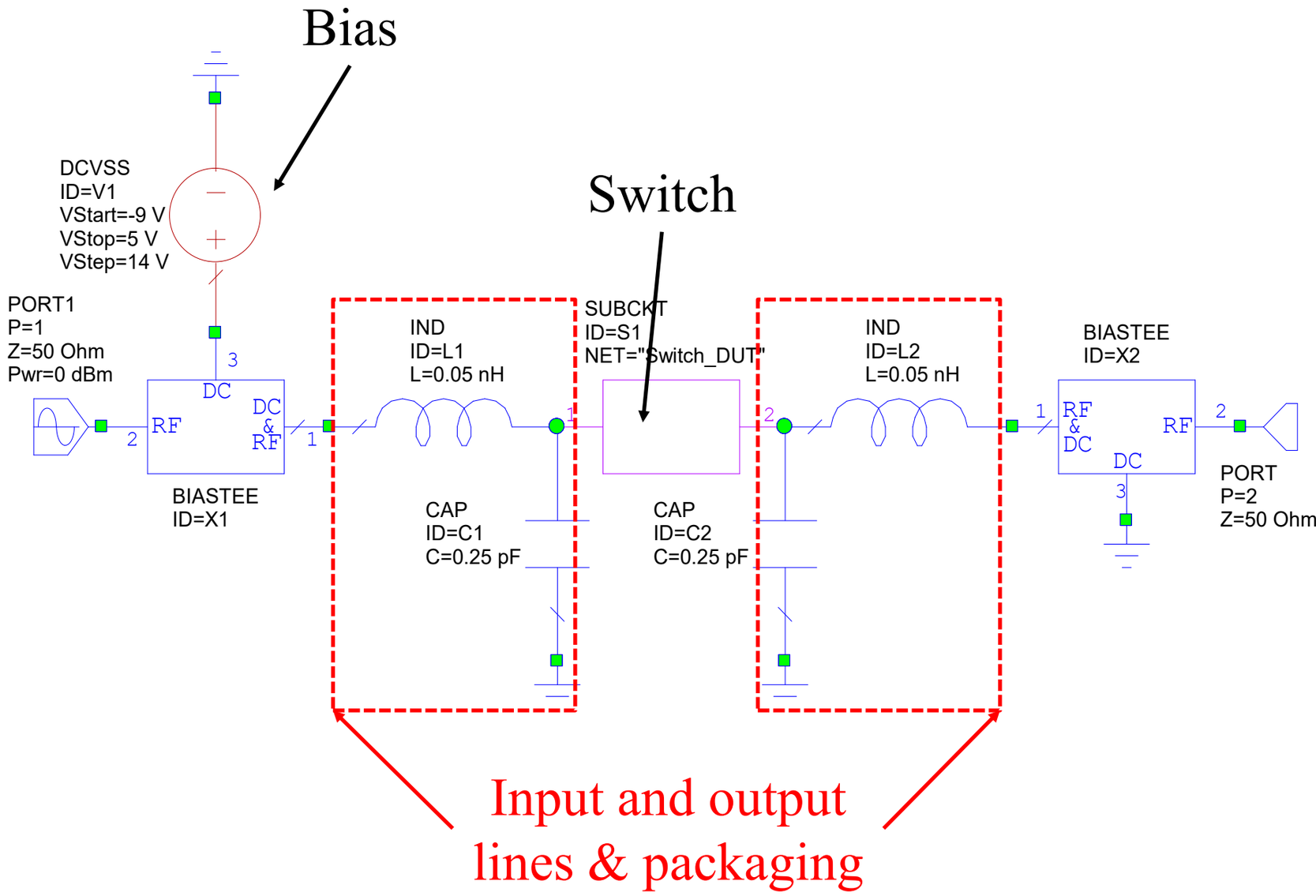
This is the author's peer reviewed, accepted manuscript. However, the online version of record will be different from this version once it has been copyedited and typeset.
PLEASE CITE THIS ARTICLE AS DOI: 10.1063/5.0151116

Journal of Applied Physics

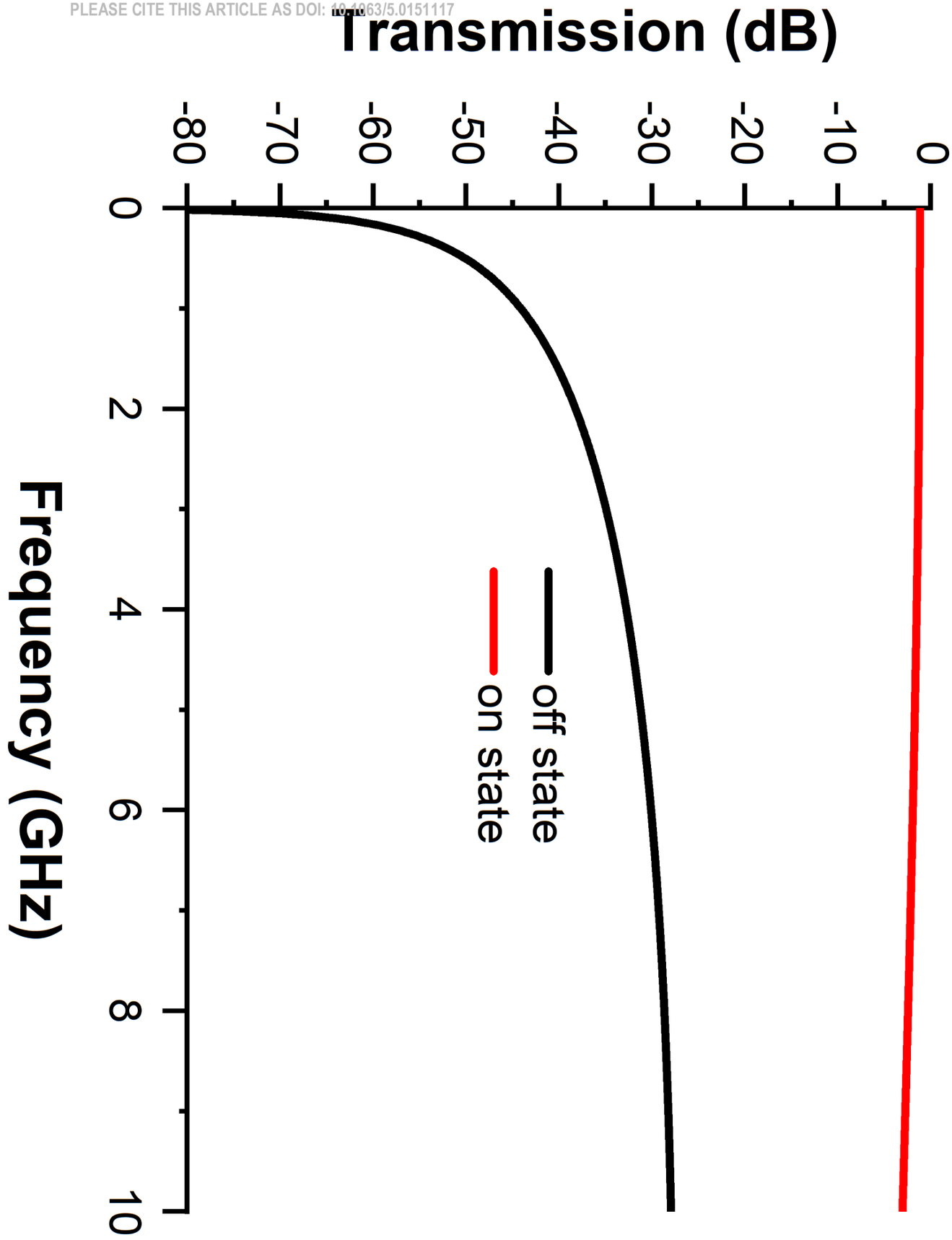
AIP Publishing



ACCEPTED MANUSCRIPT
Journal of Applied Physics
AIP Publishing
This is the author's peer reviewed, accepted manuscript. However, the online version of record will be different from this version once it has been copyedited and typeset.
PLEASE CITE THIS ARTICLE AS DOI: 10.1063/5.0151117

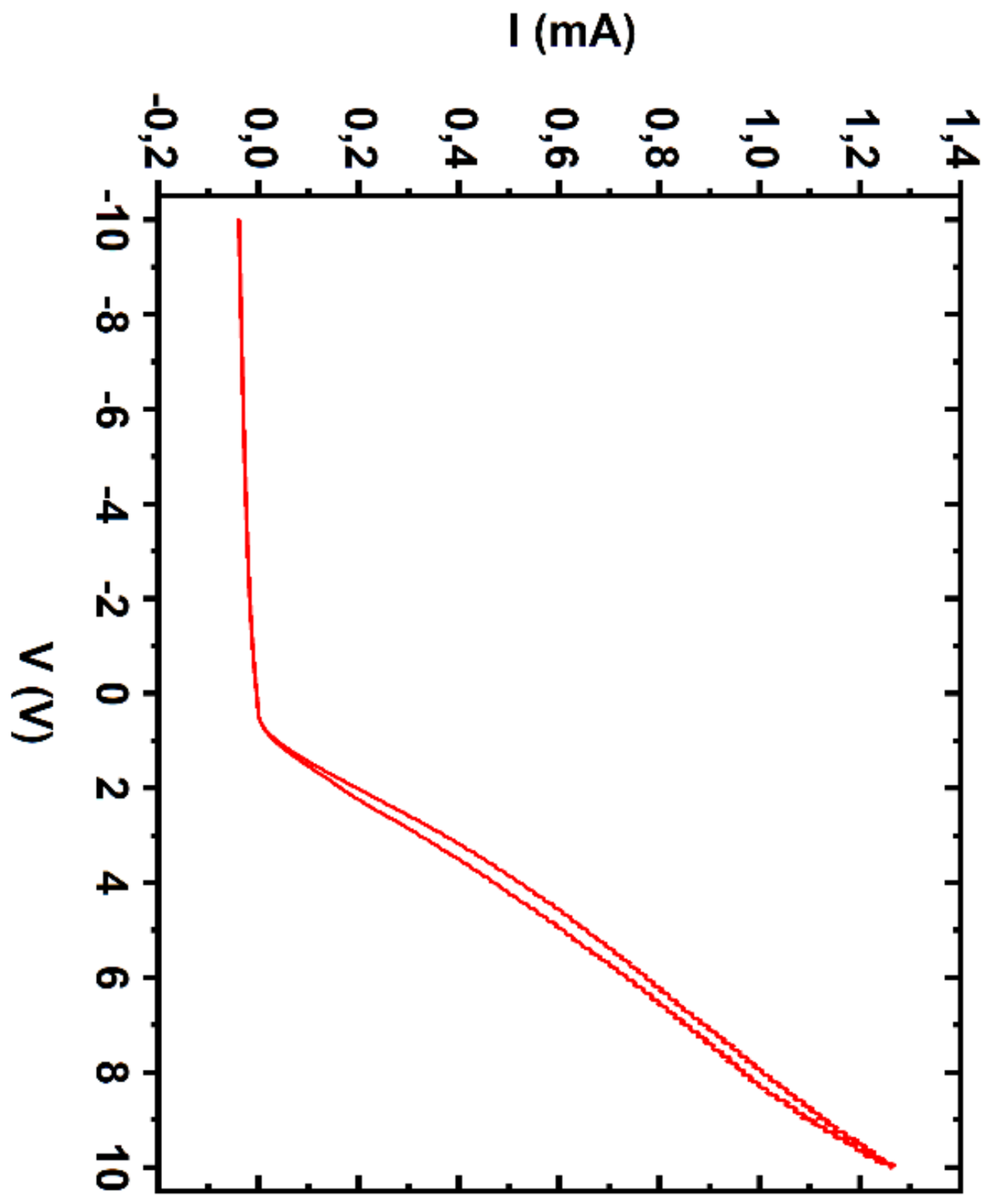


AIP Publishing
Journal of Applied Physics
ACCEPTED MANUSCRIPT
This is the author's peer reviewed, accepted manuscript. However, the online version of record will be different from this version once it has been copyedited and typeset.
PLEASE CITE THIS ARTICLE AS DOI: 10.1063/5.0151117



AIP Publishing
Journal of Applied Physics
ACCEPTED MANUSCRIPT

This is the author's peer reviewed, accepted manuscript. However, the online version of record will be different from this version once it has been copyedited and typeset.
PLEASE CITE THIS ARTICLE AS DOI: 10.1063/5.0151117

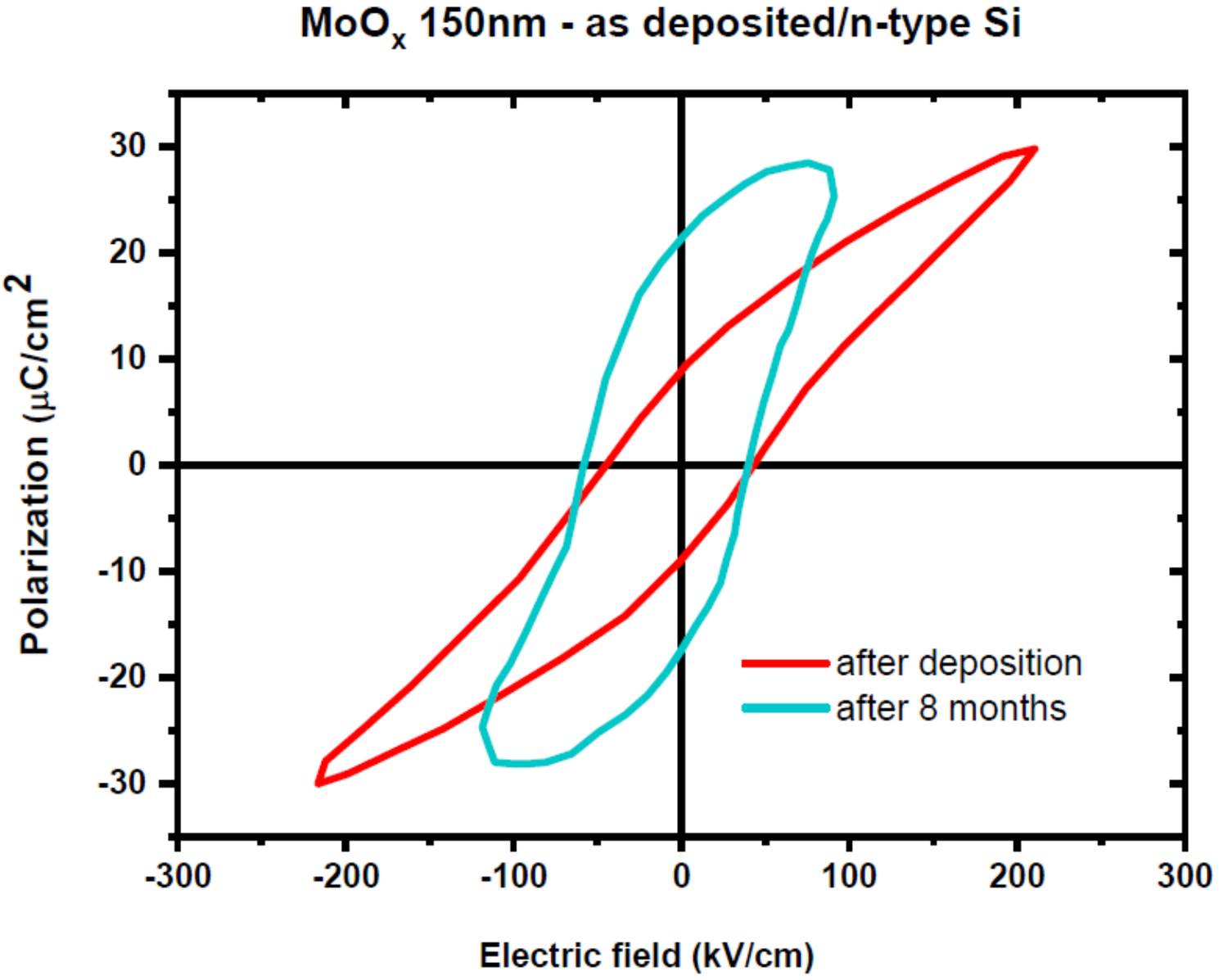


ACCEPTED MANUSCRIPT

Journal of Applied Physics

AIP Publishing

This is the author's peer reviewed, accepted manuscript. However, the online version of record will be different from this version once it has been copyedited and typeset.
PLEASE CITE THIS ARTICLE AS DOI: 10.1063/5.0151117

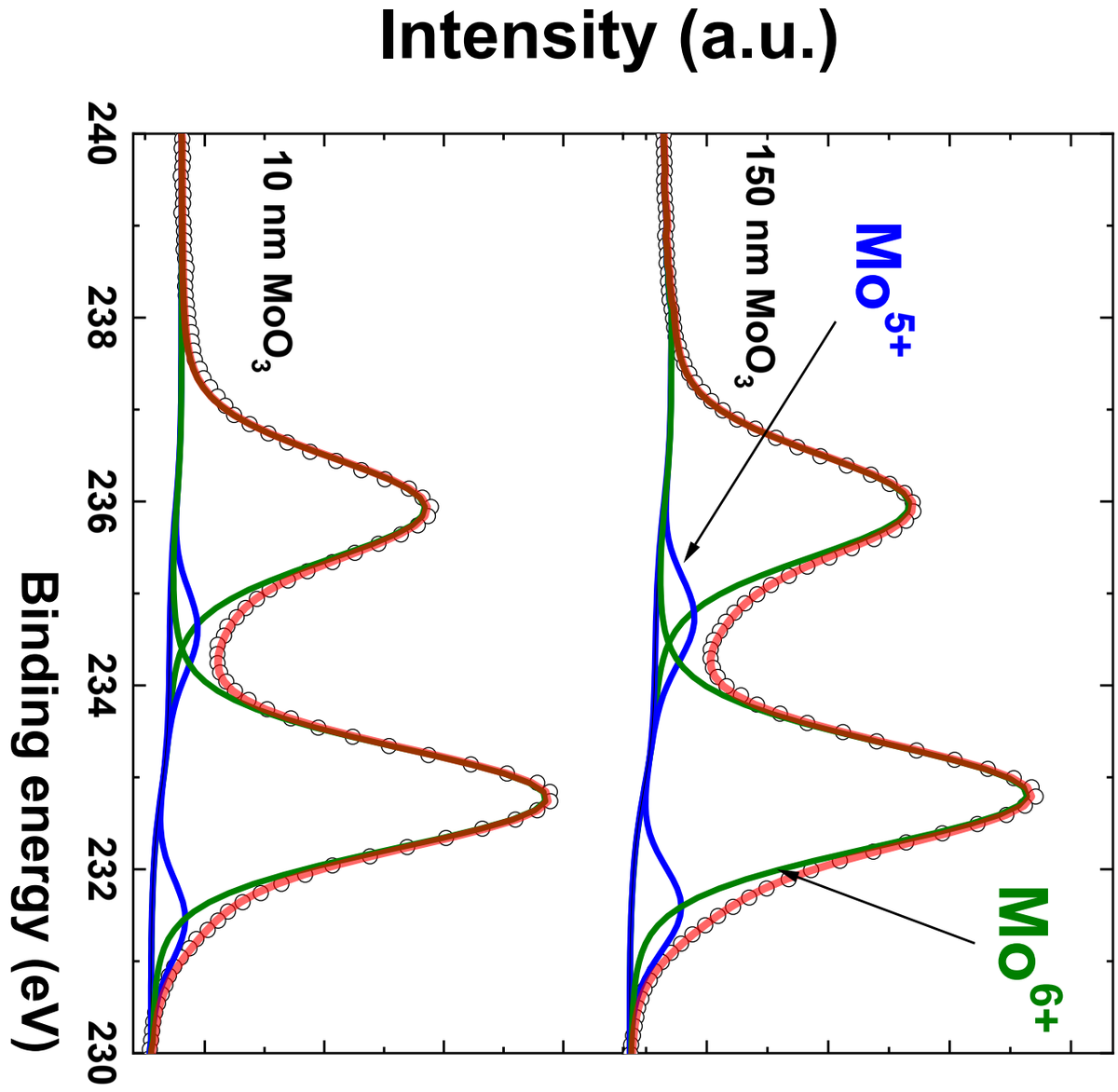


AIP Publishing

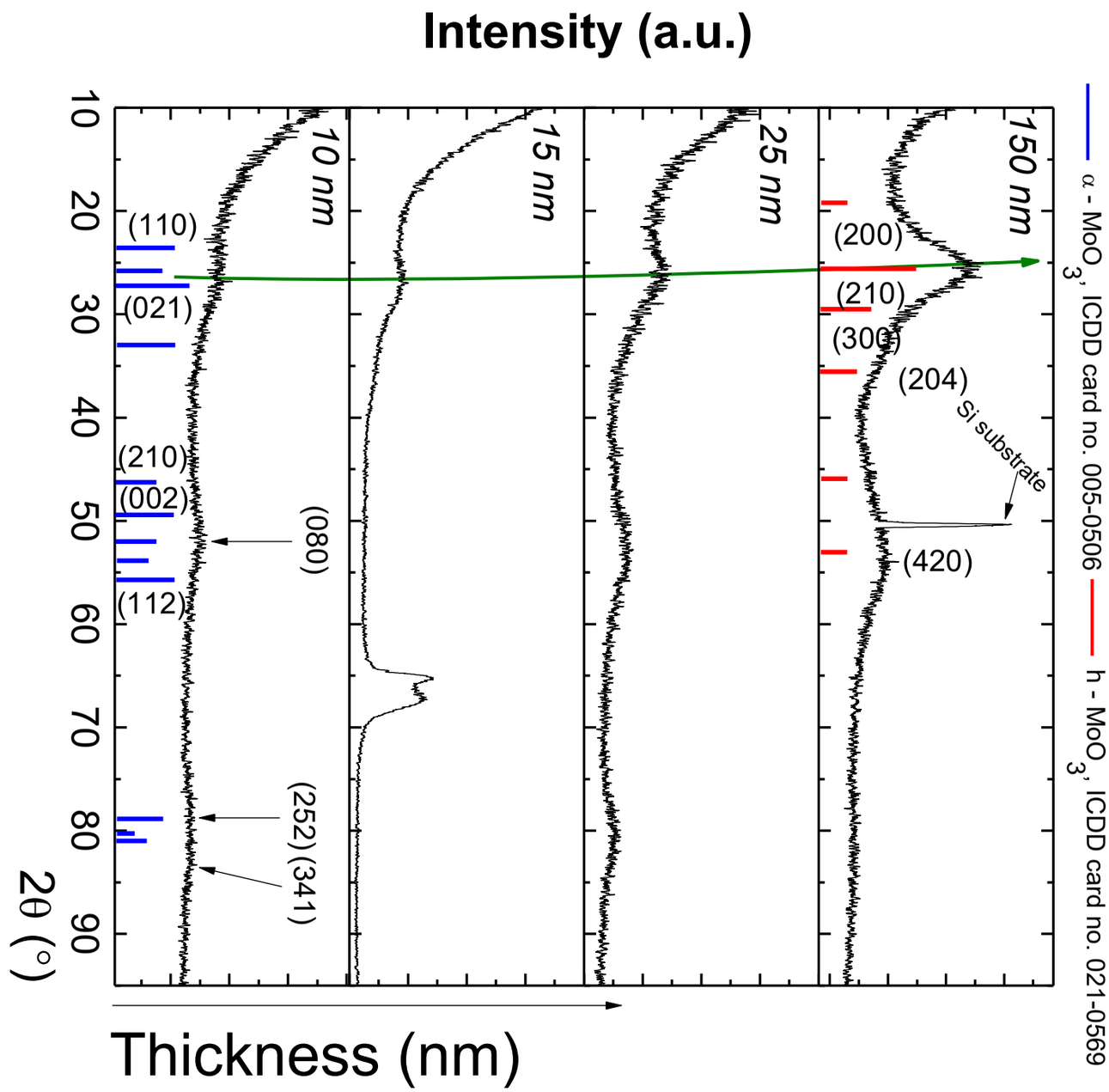
Journal of Applied Physics

ACCEPTED MANUSCRIPT

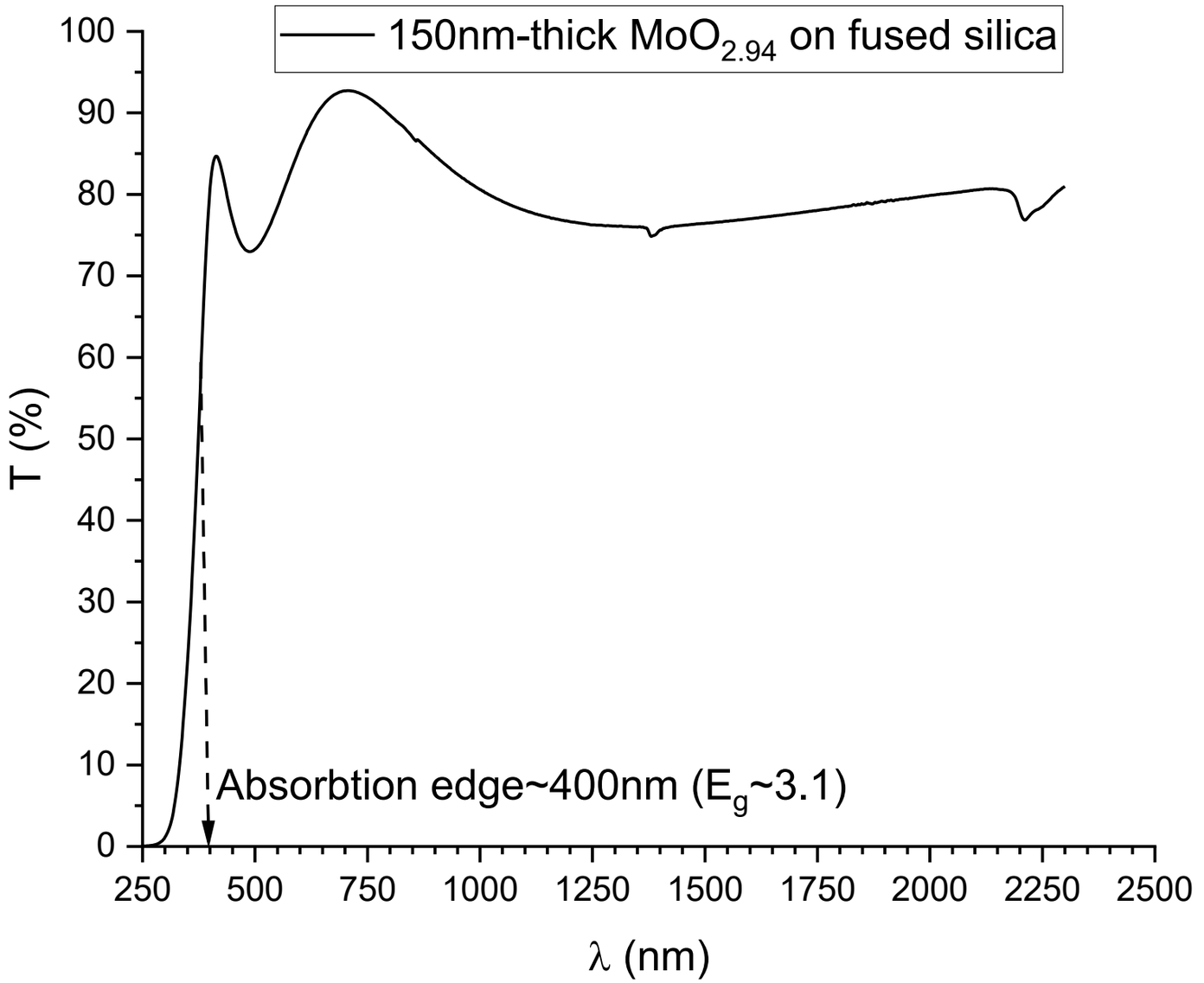
This is the author's peer reviewed, accepted manuscript. However, the online version of record will be different from this version once it has been copyedited and typeset.
PLEASE CITE THIS ARTICLE AS DOI: 10.1063/5.0151117



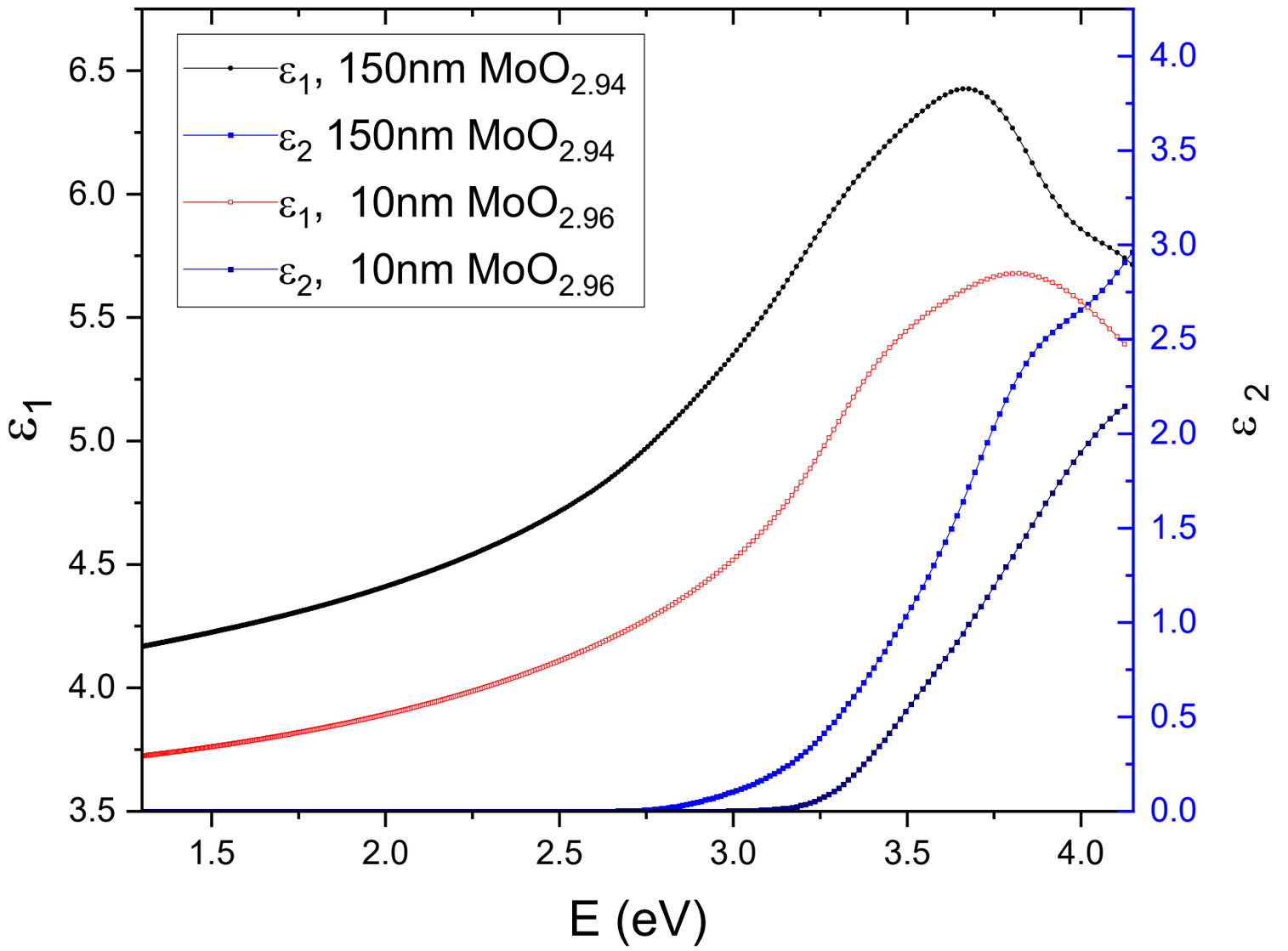
AIP Publishing
Journal of Applied Physics
ACCEPTED MANUSCRIPT
This is the author's peer reviewed, accepted manuscript. However, the online version of record will be different from this version once it has been copyedited and typeset.
PLEASE CITE THIS ARTICLE AS DOI: 10.1063/5.0151117



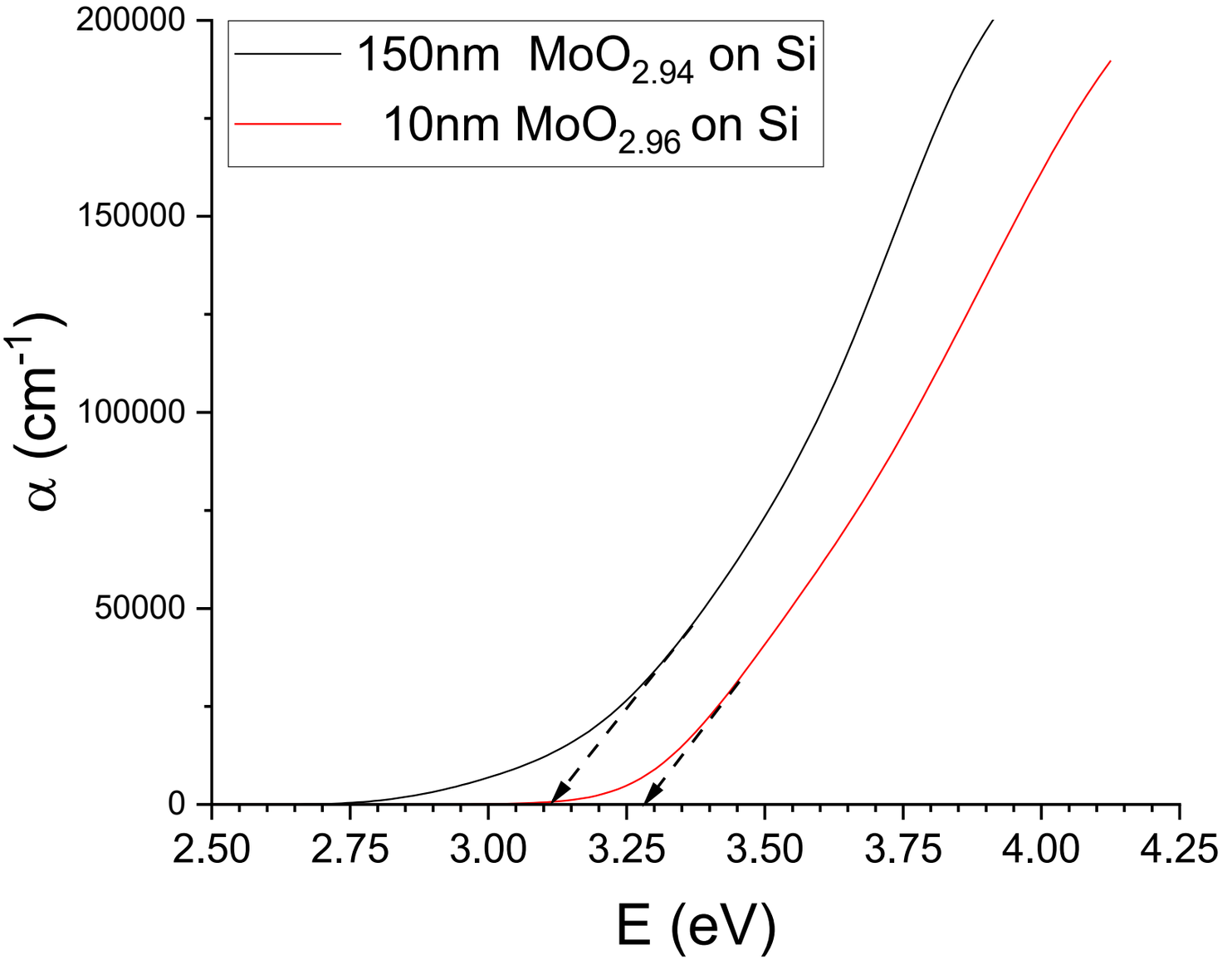
ACCEPTED MANUSCRIPT
Journal of Applied Physics
AIP Publishing
This is the author's peer reviewed, accepted manuscript. However, the online version of record will be different from this version once it has been copyedited and typeset.
PLEASE CITE THIS ARTICLE AS DOI: 10.1063/5.0151117



ACCEPTED MANUSCRIPT
Journal of Applied Physics
AIP Publishing
This is the author's peer reviewed, accepted manuscript. However, the online version of record will be different from this version once it has been copyedited and typeset.
PLEASE CITE THIS ARTICLE AS DOI: 10.1063/5.0151117



ACCEPTED MANUSCRIPT
Journal of Applied Physics
AIP Publishing
This is the author's peer reviewed, accepted manuscript. However, the online version of record will be different from this version once it has been copyedited and typeset.
PLEASE CITE THIS ARTICLE AS DOI: 10.1063/5.0151117

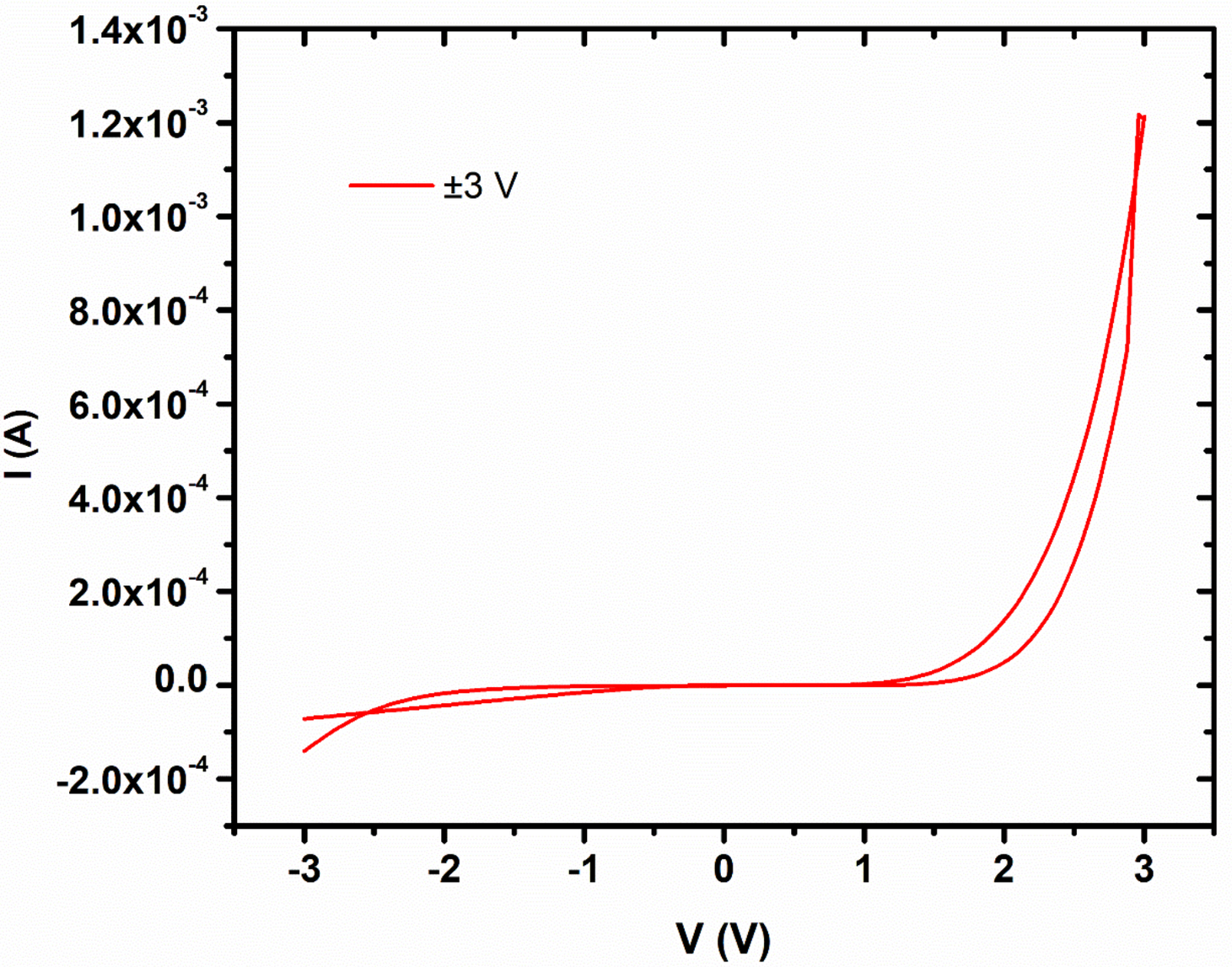


ACCEPTED MANUSCRIPT

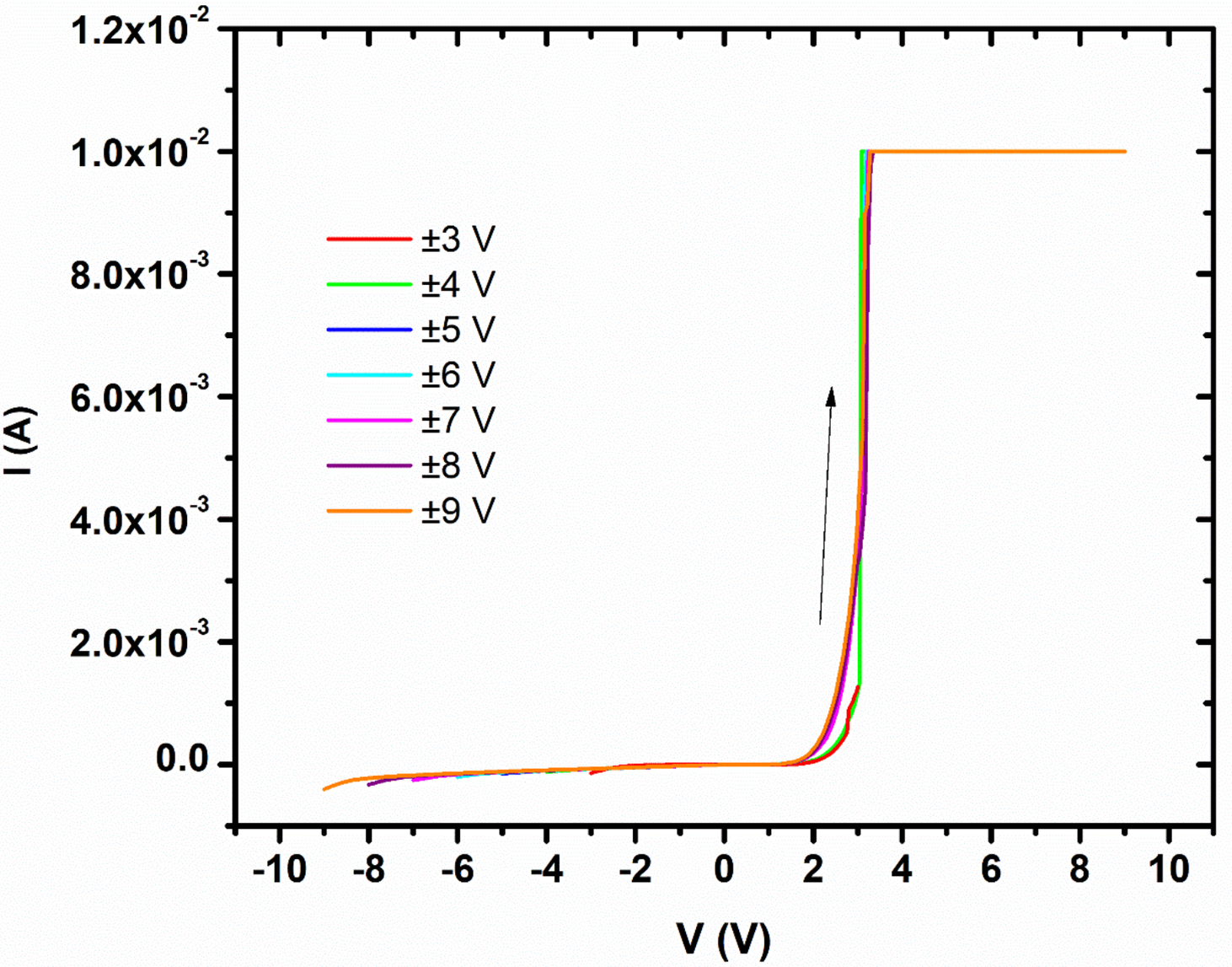
Journal of Applied Physics

AIP Publishing

This is the author's peer reviewed, accepted manuscript. However, the online version of record will be different from this version once it has been copyedited and typeset.
PLEASE CITE THIS ARTICLE AS DOI: 10.1063/5.0151117



ACCEPTED MANUSCRIPT
Journal of Applied Physics
AIP Publishing
This is the author's peer reviewed, accepted manuscript. However, the online version of record will be different from this version once it has been copyedited and typeset.
PLEASE CITE THIS ARTICLE AS DOI: 10.1063/5.0151117

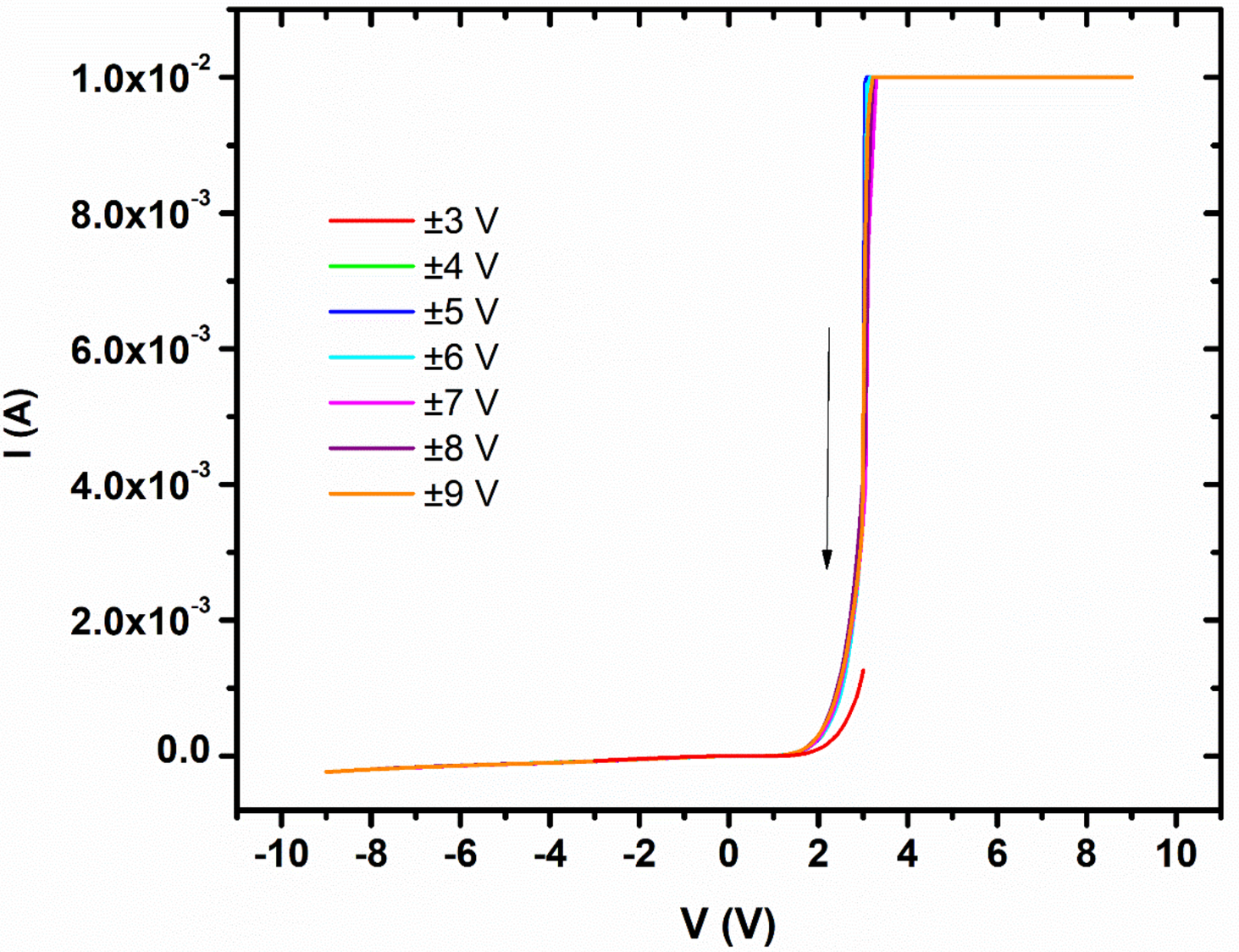


ACCEPTED MANUSCRIPT

Journal of Applied Physics

AIP Publishing

This is the author's peer reviewed, accepted manuscript. However, the online version of record will be different from this version once it has been copyedited and typeset.
PLEASE CITE THIS ARTICLE AS DOI: 10.1063/5.0151117



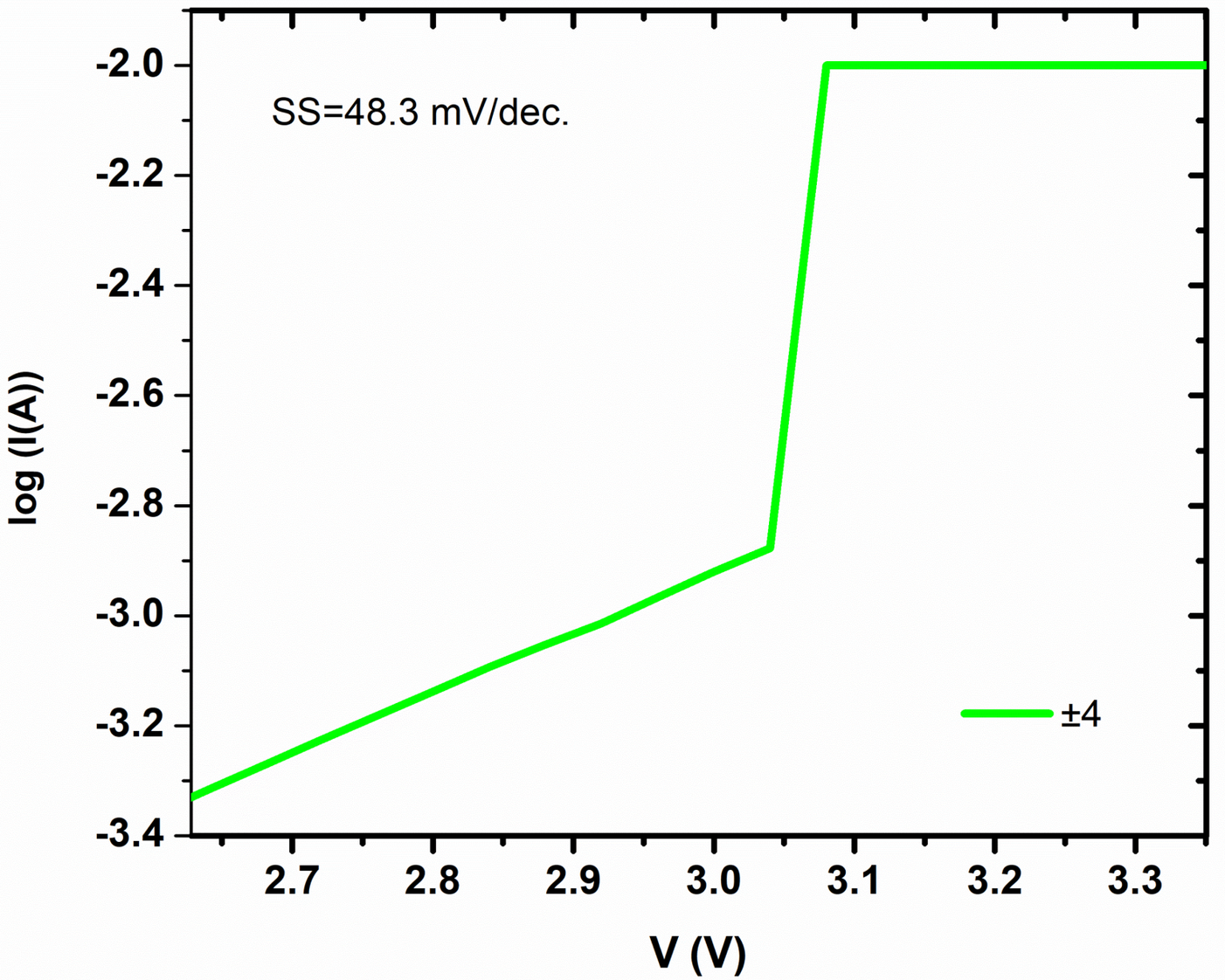
ACCEPTED MANUSCRIPT

Journal of Applied Physics

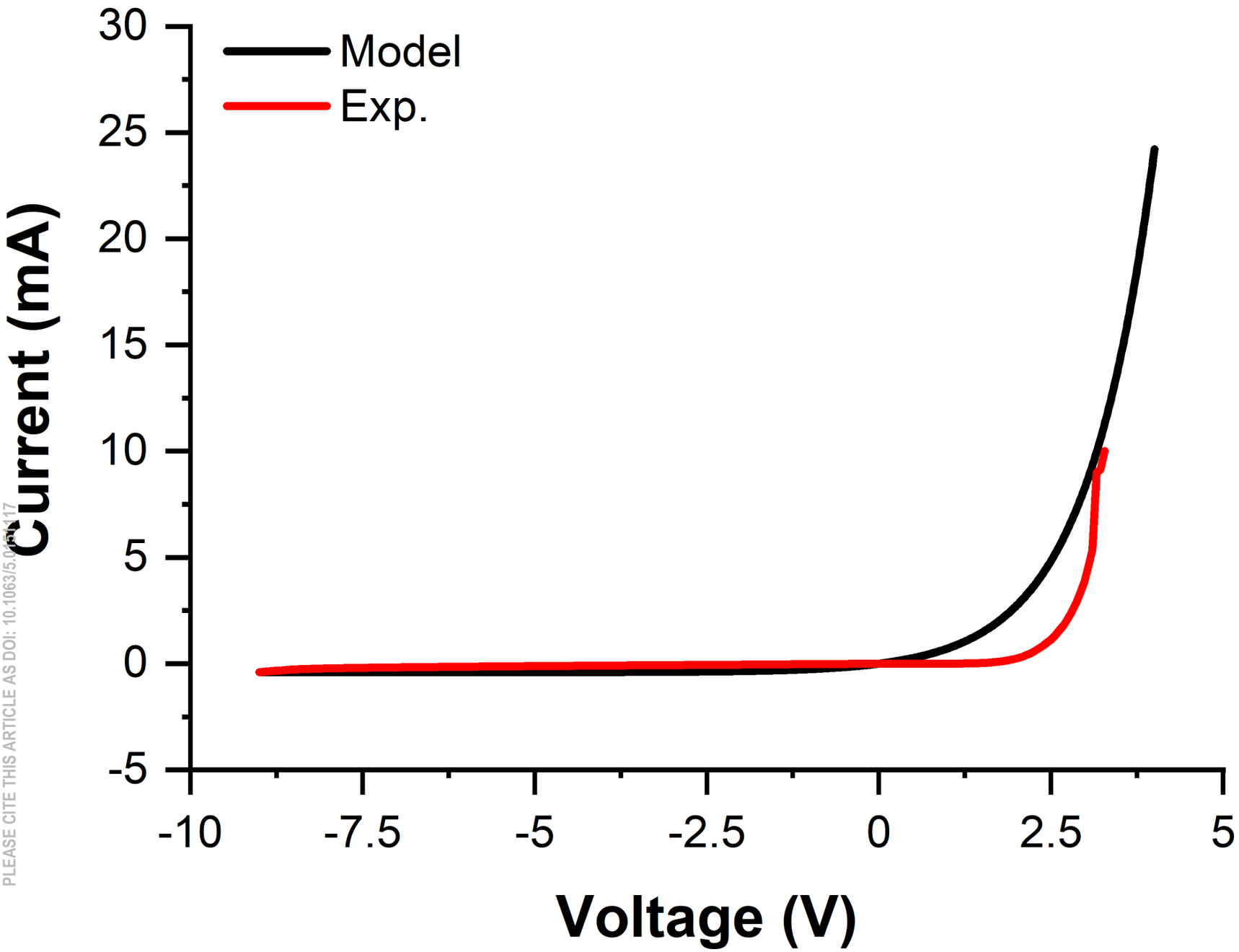
AIP Publishing

This is the author's peer reviewed, accepted manuscript. However, the online version of record will be different from this version once it has been copyedited and typeset.
PLEASE CITE

ACCEPTED MANUSCRIPT
Journal of Applied Physics
AIP Publishing
This is the author's peer reviewed, accepted manuscript. However, the online version of record will be different from this version once it has been copyedited and typeset.
PLEASE CITE THIS ARTICLE AS DOI: 10.1063/5.0151117



ACCEPTED MANUSCRIPT
Journal of Applied Physics
AIP Publishing
This is the author's peer reviewed, accepted manuscript. However, the online version of record will be different from this version once it has been copyedited and typeset.
PLEASE CITE THIS ARTICLE AS DOI: 10.1063/5.0057117

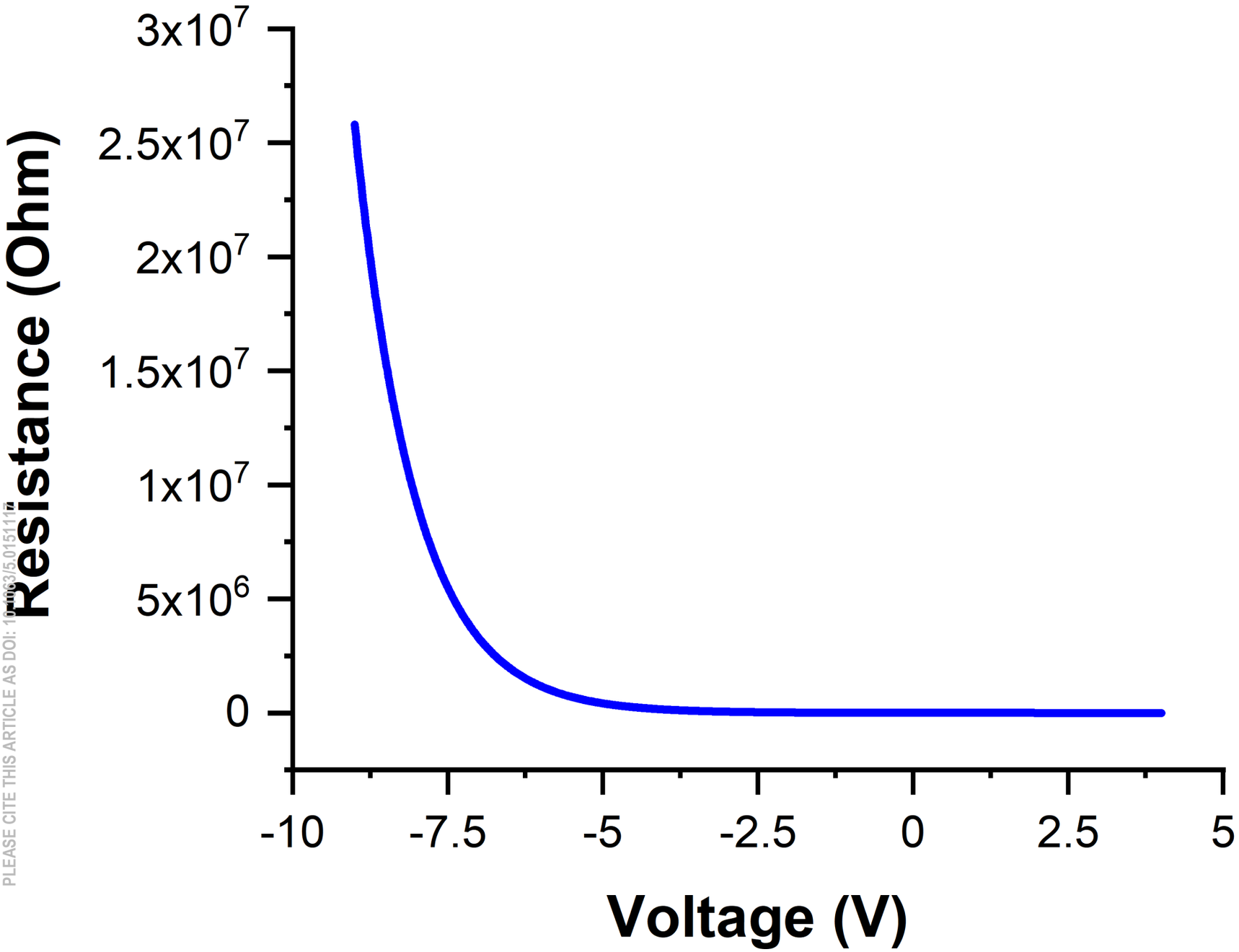


ACCEPTED MANUSCRIPT

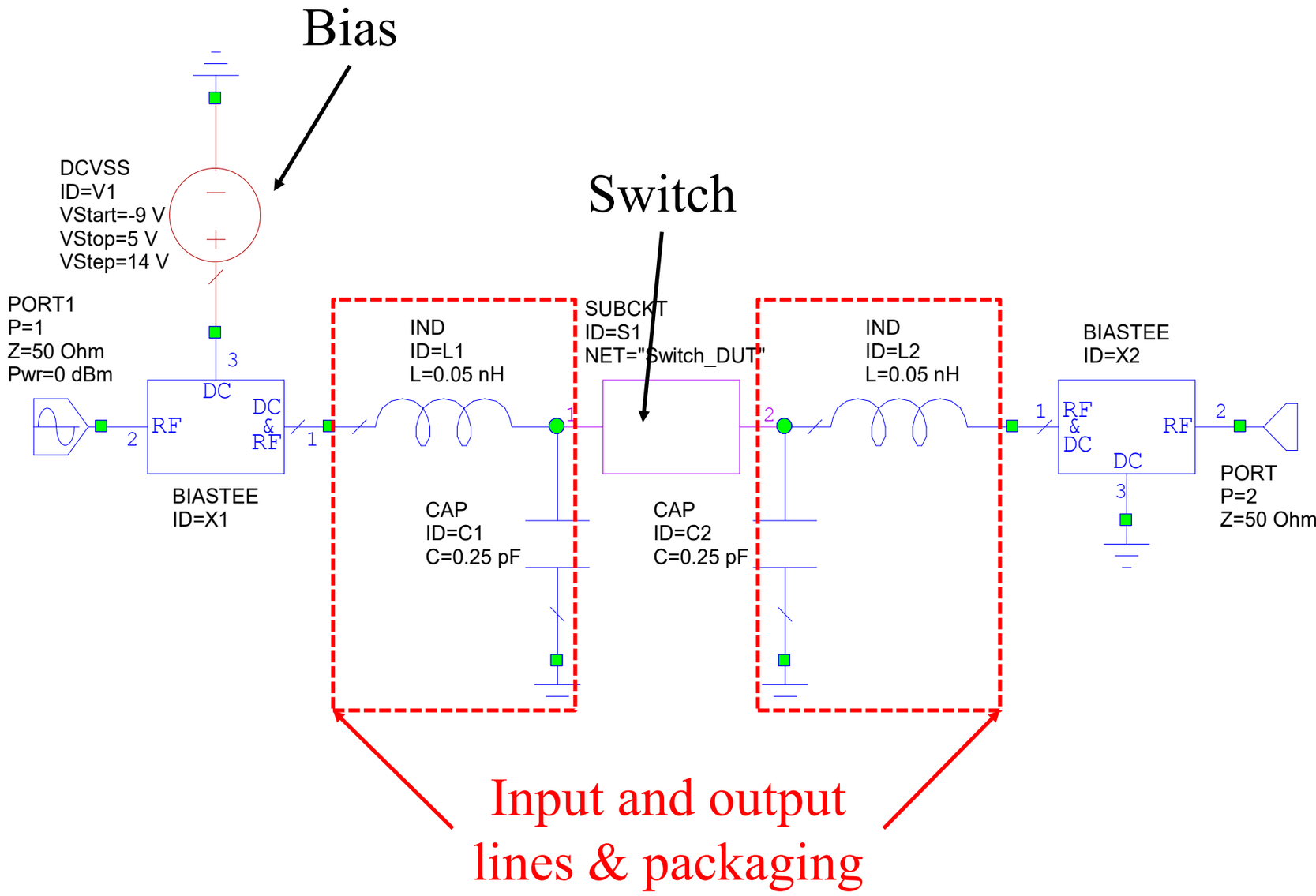
This is the author's peer reviewed, accepted manuscript. However, the online version of record will be different from this version once it has been copyedited and typeset.
PLEASE CITE THIS ARTICLE AS DOI: 10.1063/5.0151116

Journal of Applied Physics

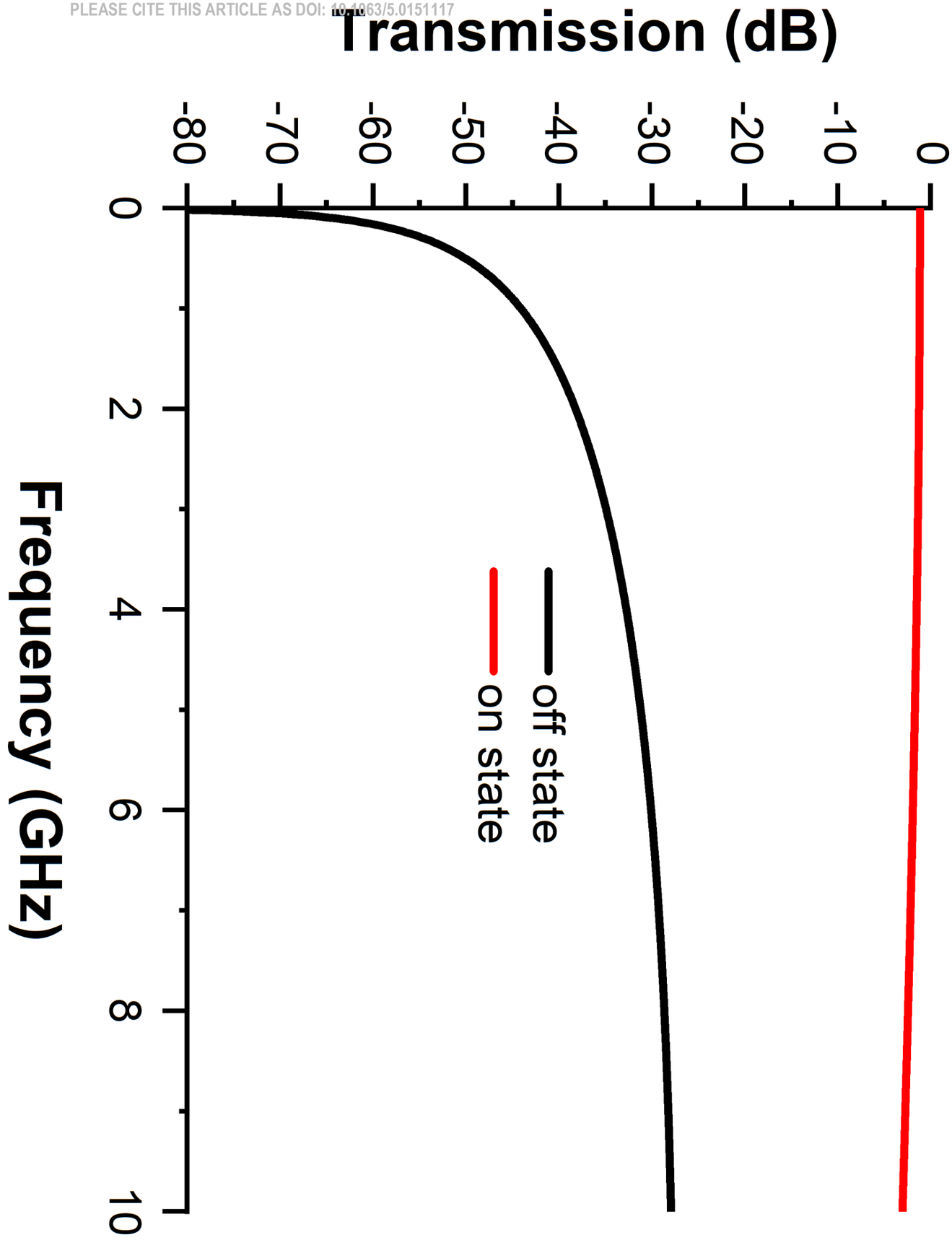
AIP Publishing



ACCEPTED MANUSCRIPT
Journal of Applied Physics
AIP Publishing
This is the author's peer reviewed, accepted manuscript. However, the online version of record will be different from this version once it has been copyedited and typeset.
PLEASE CITE THIS ARTICLE AS DOI: 10.1063/5.0151117



AIP Publishing
Journal of Applied Physics
ACCEPTED MANUSCRIPT
This is the author's peer reviewed, accepted manuscript. However, the online version of record will be different from this version once it has been copyedited and typeset.
PLEASE CITE THIS ARTICLE AS DOI: 10.1063/5.0151117

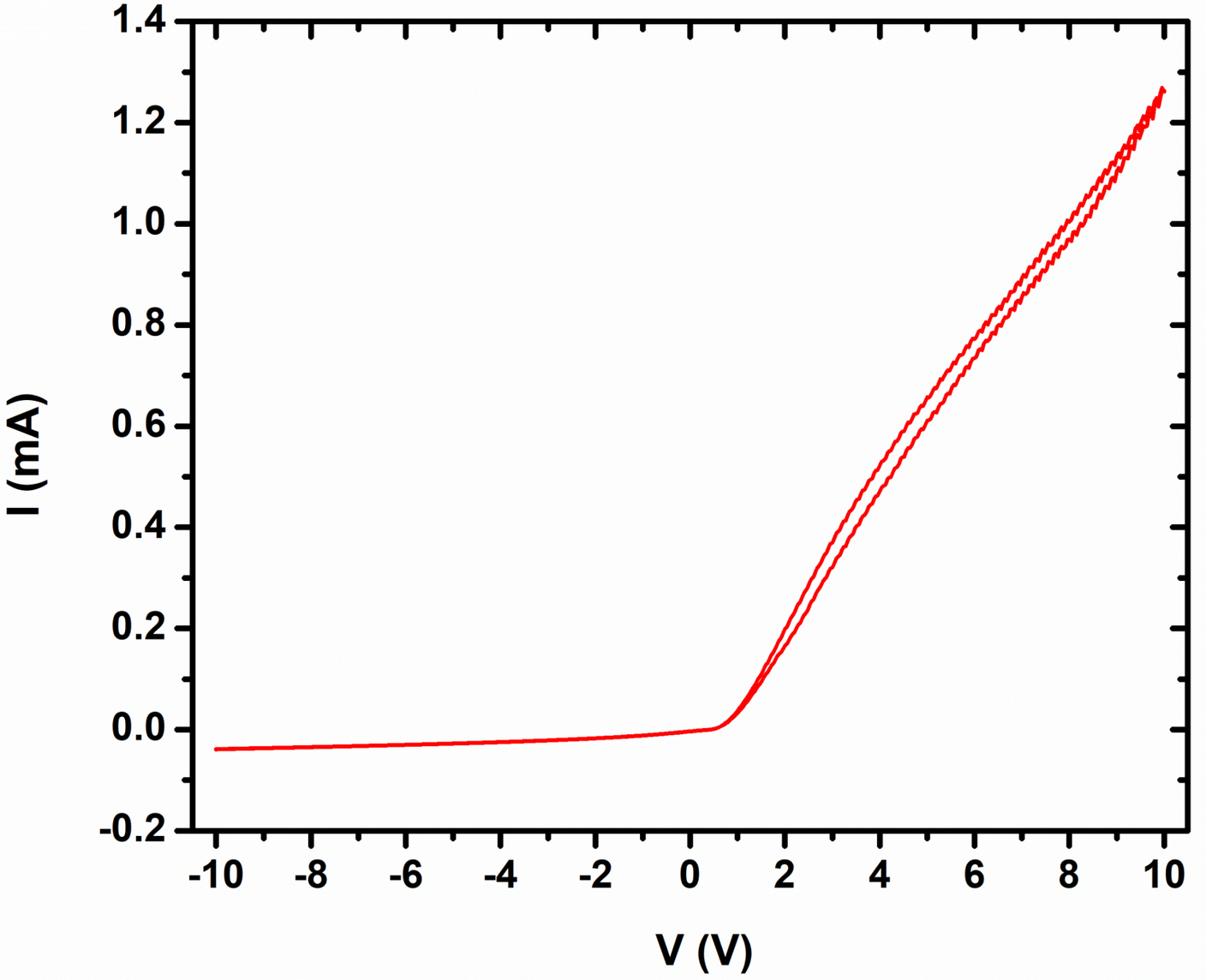


ACCEPTED MANUSCRIPT

Journal of Applied Physics

AIP Publishing

This is the author's peer reviewed, accepted manuscript. However, the online version of record will be different from this version once it has been copyedited and typeset.
PLEASE CITE THIS ARTICLE AS DOI: 10.1063/5.0151117



ACCEPTED MANUSCRIPT

Journal of Applied Physics

AIP Publishing

This is the author's peer reviewed, accepted manuscript. However, the online version of record will be different from this version once it has been copyedited and typeset.
PLEASE CITE THIS ARTICLE AS DOI: 10.1063/5.0151117

